HIGH RESOLUTION SUBMILLIMETER WAVE SPECTROSCOPY OF HBr, DBr AND HI

F. A. VAN DIJK

HIGH RESOLUTION SUBMILLIMETER WAVE SPECTROSCOPY OF HBr, DBr AND HI

PROMOTOR: PROF. DR. A. DYMANUS

HIGH RESOLUTION SUBMILLIMETER WAVE SPECTROSCOPY OF HBr, DBr AND HI

PROEFSCHRIFT

TER VERKRIJGING VAN DE GRAAD VAN DOCTOR
IN DE WISKUNDE EN NATUURWETENSCHAPPEN AAN DE
KATHOLIEKE UNIVERSITEIT TE NIJMEGEN, OP GEZAG VAN
DE RECTOR MAGNIFICUS DR. G. BRENNINKMEIJER,
HOOGLERAAR IN DE FACULTEIT DER SOCIALE WETENSCHAPPEN,
VOLGENS BESLUIT VAN DE SENAAT IN HET OPENBAAR TE
VERDEDIGEN OP DONDERDAG 23 SEPTEMBER 1971
DES NAMIDDAGS TE 4 UUR

DOOR

FRANCISCUS ALBERTUS VAN DIJK

geboren te Lemmer

1971
DRUKKERIJ GEBR. JANSSEN N.V. NIJMEGEN

Aan het begin van dit proefschrift wil ik allen bedanken, die bijgedragen hebben in het tot stand komen ervan. Enkelen wil ik in het bijzonder vermelden.

Dr. C. Huiszoon, die mij heeft ingewijd in de experimentele technieken van dit onderzoek.

De heer F. van Rijn voor de uitstekende technische hulp gedurende het hele onderzoek.

Dr. J. Reuss en Dr. J. Verhoeven voor de vele verhelderende discussies.

De heren H. Bogers, Drs. P. van Overbeek, J. Ragas en Drs. B. Zuidberg voor het vele werk dat zij tijdens hun afstudeerperiode aan dit onderzoek verricht hebben.

De leden van de werkgroep Atoom- en Molekuulfysika voor de prettige samenwerking.

De dienst verlenende afdelingen wil ik graag bedanken in de personen van de Heren J. van Langen, M. van der Kop en W. van Royen.

De illustraties in dit proefschrift werden verzorgd door de afdeling illustratie onder leiding van de Heer J. Gerritsen.

Aan mijn ouders
Aan Thea

CONTENTS

CHAPTER I

INTRODUCTION

I.1 SPECTROSCOPY IN THE SUBMILLIMETER REGION

Spectroscopic research is an important source of information concerning structure of atoms and molecules. Molecular spectra cover a broad region of the electromagnetic spectrum, from the ultraviolet to radio frequencies. A part of this spectrum in which so far relatively little research has been done is the region extending from short millimeter waves ($\lambda \sim 2$ mm) to far infrared ($\lambda \sim 0.1$ mm). This region is often called the submillimeter region. The rather low spectroscopic activity in this region is due to lack of sources of sufficient power, bandwidth and stability. However, it is a very interesting region for molecular physics, because many molecules have transitions in it. Also in solid state physics energies corresponding to radiation in this region are of frequent occurence; for example, the characteristic energy gap of the correlated pairs of superconducting electrons.

The spectroscopic techniques for the submillimeter region are borrowed either from microwaves with electron-beam sources (klystrons, backward-wave oscillators), harmonic generators, waveguides, etc. or from the infrared region, with broadband thermal or discharge sources (mercury-arc lamp) and optical devices such as mirrors, diffraction gratings, interferometers (MAR 67). The research possibilities of these techniques are seriously hampered both by low sensitivity and by low intrinsic resolution of the spectrometers.

With grating and Fourier transform spectrometers equipped with broadband thermal sources a resolution of 0.05–0.1 cm^{-1} has been obtained for wavelengths longer than 150 μm (wavenumber smaller than 67 cm^{-1}) (KNE 69). Using microwave techniques Gordy and coworkers have measured spectral lines of HCl, CO and NH_3 in the 0.4–0.6 mm region (JON 64a, b; HEL 69) with a 30 cm long G-band absorption cell fed by radiation from harmonic generators driven by klystrons. Most recently they have measured rotational transitions of CO and OCS at about 0.37 mm (HEL 70). The halfwidth (at half of the maximum intensity) in these experiments was 0.5–1.0 MHz.

The resolution of the latter kind of spectrometers is better than the resolution of grating spectrometers and interferometers. However, it is insufficient to resolve most of the hyperfine structure (hfs) of molecular transitions in the submillimeter region. An important step forward was development of the high resolution beam-absorption spectrometer by Huiszoon (HUI 66a, 66b, 71).

With this spectrometer a resolution of about 5 kHz has been obtained in the frequency region of 150–300 GHz. One of the goals of the present investigation was to extend this technique into the region of 500–700 GHz. As will be shown in Chap. 2 the highest frequency at which sufficient power can be generated for beam-absorption spectroscopy using present detection techniques is estimated to be about 800 GHz.

New possibilities for spectroscopy with high resolution in the submillimeter region can be expected by using lasers. Indispensable for spectroscopy is a tunable range of frequencies with sufficient power, and for high resolution spectroscopy a high stability and spectral purity of the radiation source. By Corcoran *et al* (COR 70) sum and difference frequency signals have been generated by mixing the outputs of a CO_2 infrared laser and of a tunable millimeter wave klystron in a gallium-arsenide crystal mounted in a waveguide. These investigators (CUP 70) also succeeded in phase-locking of the 890 GHz (0.34 mm) radiation of an HCN laser to a frequency standard. As a result, coherent frequency stable signals tunable over the tuning range of a klystron will become available in the submillimeter region.

1.2 THE MOLECULAR BEAM SPECTROMETER

Crystal harmonic generators driven by klystrons phase-locked to a frequency standard are sources of an essentially monochromatic radiation in the submillimeter region. At low gas pressures the resolution of an absorption-cell spectrometer is then determined ultimately by the Doppler broadening of the spectral lines.

For a gas with Maxwellian velocity distribution the halfwidth $\Delta\nu_D$ of a spectral line due to the Doppler broadening is (TOW 55, p. 337):

$$\Delta\nu_D = \frac{\nu}{c}\sqrt{2kN_0\ln 2}\,\sqrt{T/M} = 3.581 \times 10^{-7}\sqrt{T/M}\,\nu \qquad (1.1)$$

where ν is the frequency of the line, c velocity of light, k the Boltzmann constant, N_0 the Avogadro number, M the molecular weight, and T the absolute temperature. As an example, the Doppler halfwidth of the HBr line at 500 GHz is 350 kHz for the gas at room temperature.

In the spectrometer of Huiszoon (HUI 66b, 71) high resolution is obtained by reducing the Doppler broadening with a factor of 50 by using molecular beam techniques. A detailed description of the spectrometer of Huiszoon can be found in references mentioned above. Only a general outline of the spectrometer is given below.

The principle of the molecular beam spectrometer, in which reduction of Doppler broadening is achieved by letting the absorbing molecules to travel perpendicularly to the direction of propagation of the microwave radiation, is shown in Fig. 1.1. The absorption cell of the spectrometer consists of two

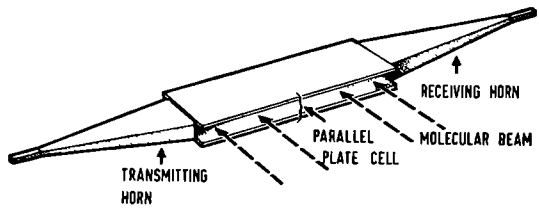

FIG. 1.1 The absorption cell with horns. The direction of the molecular beam is indicated by arrows (from: C. Huiszoon, 'High resolution millimeter wave spectroscopy' (HUI 66b)).

electrically isolated flat copper plates. The plates are 40 cm long, 10 cm wide and their mutual separation is 1 cm. The plates serve both as a transmission system for the microwaves and as a means for applying a Stark field. The microwave radiation is sent between the plates in the longitudinal direction by a transmitting horn and received by an identical horn. The propagation mode is essentially TEM with the microwave E-vector perpendicular to the plates. The absorbing molecules travel as a well collimated beam between the parallel plates in a direction perpendicular to the direction of propagation of the microwaves. The beam of molecules is obtained with the aid of a diaphragm placed between the effuser and the parallel-plate cell. This diaphragm is kept at liquid nitrogen temperature and serves to trap molecules which would otherwise make collisions with the plates and be scattered, or which would travel along paths deviating too much from the direction perpendicular to the radiation path. After travelling through the parallel-plate cell region the beam is trapped in a liquid nitrogen condenser.

To obtain good sensitivity a superheterodyne detection scheme is used together with low frequency square wave Stark modulation and phase sensitive detection. The modulating voltage is applied between the plates of the cell. At the same time a d.c. voltage can be applied between the plates to measure the dipole moments of molecules.

After the reduction of the Doppler broadening other effects can determine the ultimate line width. For the beam spectrometer these are the Heisenberg broadening and broadening as a result of frequency fluctuations of the signal oscillator. The latter broadening is kept very small (< 2 kHz) by the electronic

locking of the signal klystron to the frequency standard. The Heisenberg broadening follows from

$$2\Delta\nu_H\Delta t \cong 1 \tag{1.2}$$

where $\Delta\nu_H$ is the halfwidth of the line due to Heisenberg broadening, and Δt is the mean transit time of the molecules through the absorption cell. For the transition of HBr at 500 GHz and with a molecular path through the radiation field of 10 cm, a value of 1.7 kHz is obtained for $\Delta\nu_H$ for gas at room temperature. However, the value of the residual Doppler broadening for the same line equals 7.0 kHz, as follows from Eq. (1.1) and the reduction factor of 50.

1.3 THE PRESENT INVESTIGATION

As stated above the primary goal of the present investigation was extension of the high resolution spectroscopy into the 300–700 GHz region. With the available high resolution hyperfine and other properties of a number of diatomic molecules, which are not readily accessible to other experimental techniques, are measured. The results are discussed in terms of electronic and structural models of the molecules.

The spectrometer used in the present investigation is essentially that of Huiszoon (HUI 66b) apart from harmonic generation and detection of submillimeter radiation. Typical resolution of this molecular beam spectrometer is 3–7 kHz, determined mainly by residual Doppler broadening. Its range is from about 100 to about 700 GHz.

The submillimeter waves are obtained from a klystron driven crystal harmonic generator. The techniques of generation and detection of short millimeter and submillimeter waves and of frequency stabilization and measurement are described in Chap. 2.

Spectroscopic measurements have been performed on the rotational transition $J = 0 \rightarrow 1$ of the molecules HI and HBr at 385 GHz and 500 GHz, respectively. The resolution is sufficiently high to resolve completely the electric and magnetic hyperfine structure of these transitions. The measurements on HBr are done for $H^{79}Br$ and $H^{81}Br$, both in natural abundance of 50 %. To investigate the influence of the isotopic substitution of H by D, the rotational transition $J = 0 \rightarrow 1$ of the molecules $D^{79}Br$ and $D^{81}Br$ at 254 GHz was also measured.

The molecular constants which are obtained from the hyperfine spectra, are the rotational constant B_0, the electric quadrupole coupling constant of i-th nucleus $(eqQ)_i$, the spin-rotation coupling constant of i-th nucleus C_1, and the

tensorial spin-spin coupling constant d_T. From the Stark spectra of these molecules the electric dipole moment is obtained with high accuracy.

The Hamiltonian used for the interpretation of the spectra is given in Chap. 3. The experimental results on spectra and molecular constants are given in Chap. 4.

The molecules HF, DF, $H^{35}Cl$ and $D^{35}Cl$ have been measured with the molecular beam electric resonance (MBER) method by Muenter (MUE 70), Kaiser (KAI 70), and De Leeuw (LEE 71). With the measurements on the molecules $H^{127}I$, $H^{79}Br$, $H^{81}Br$, $D^{79}Br$, and $D^{81}Br$ the above mentioned molecular constants are now known for the four first hydrogen-halides and the three first deuterium-halides. In Chap. 4 the present results are compared with results of other investigators. In Chap. 5 the results are discussed in terms of electronic properties of the molecules.

GENERATION AND DETECTION OF SUBMILLIMETER WAVE POWER

2 1 THE HARMONIC GENERATION

The harmonic generators used in the present experiment were of the cross-waveguide configuration. Two models were used differing in the constructional details and dimensions of the in- and output waveguides. One model built by Huiszoon (HUI 66b) is a slight modification of the design of Ohl, Budenstein and Burrus (OHL 59) The generator is driven by a 60 GHz klystron (OKI, 60V10) with a power output of about 100 mW. The primary waveguide has 3.10 × 1 55 mm ID (RG-99/U), with a low frequency cut-off at 48 GHz. The output waveguide has 1 65 × 0.825 mm ID (RG-136/U), with a low frequency cut-off at 90 GHz A cross-sectional view of this harmonic generator is shown in Fig. 2.1.

The multiplying crystal of the harmonic generator is mounted on a brass pen. It is brought into the crossed waveguide from the primary waveguide through the hole in the partition between the two waveguides (Fig. 2 2a). The dimensions of the hole are a compromise between conflicting requirements. A small hole is required for low leakage of harmonics to the primary waveguide. On the other hand the resulting capacity between the crystal pen and the wall separating the two waveguides must not be large enough to prevent fundamental power reaching the crystal If the whisker is put through the two waveguides with the crystal in the wall of the primary waveguide (Fig 2 2b), then the whisker

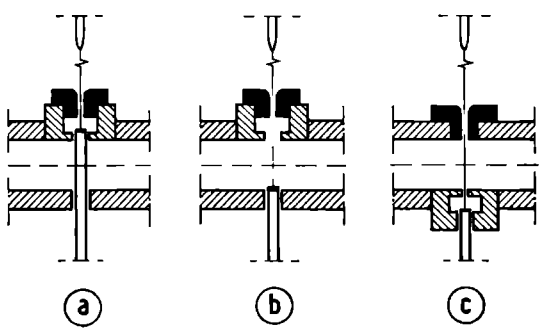

FIG. 2 2 Mounting of the point-contact diode in the crossed-waveguide harmonic generator

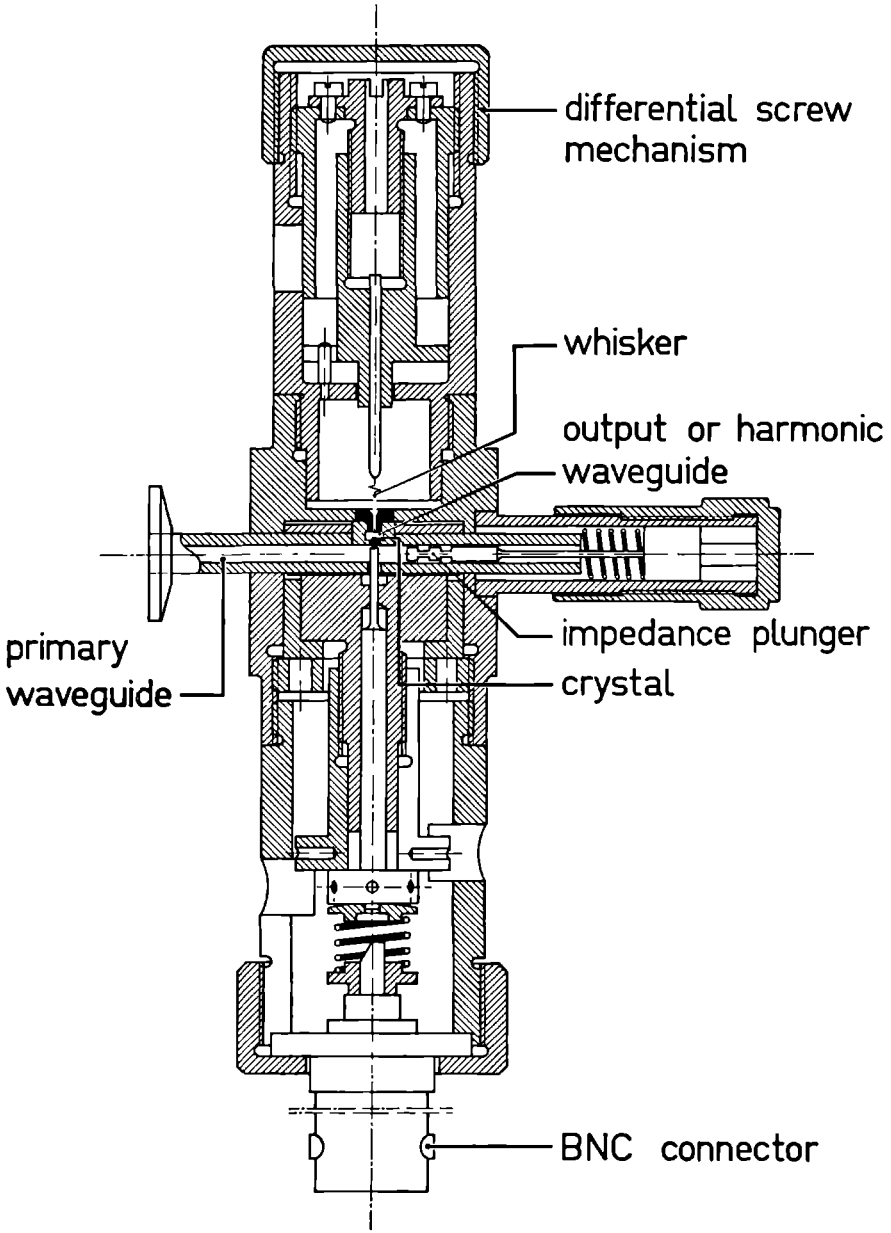

FIG. 2.1 Cross-sectional view of the harmonic generator.

sends a great deal of the higher harmonic power into the larger waveguide. A solution of this problem lies in the interchange of the whisker and the crystal-pen (Fig. 2.2c). This is done in the new model of generator used in the present experiment.

The second generator is driven by a 100 GHz klystron (Varian, VC735) with a power output of 100–200 mW. The primary waveguide has 2.54 × 1.27 mm ID. This waveguide is good for frequencies between 75 and 110 GHz; its cut-off frequency is 59 GHz. The output waveguide has 1.65 × 0.825 mm ID and a cut-off frequency of 90 GHz. The output waveguide was reduced to 1.09 × 0.55 mm ID (RG-137/U), with cut-off frequency at 137 GHz. These waveguides have been electroformed. The crystal has been placed in the narrow part of the waveguide.

The crystals used in both harmonic generators are boron doped silicon crystals bombarded with carbon ions (OHL 59). The whisker is a tungsten wire of 0.05 mm diameter sharpened to a point. The contact area has a radius of about 1 μm. The diode characteristics of a tungsten point-contact on boron doped silicon with different surface treatments are given by Ohl *et al* (OHL 59), and by Burrus (BUR 64). The method of operation is as described by Huiszoon (HUI 66b) and by Ohl. A reverse d.c. bias shifts the operating point to the reverse breakdown of the crystal characteristics. The microwave power is then turned on, and the bias voltage is readjusted to provide the maximum harmonic output.

With these harmonic generators frequencies of 385 GHz and 500 GHz with sufficient power for molecular beam spectroscopy (10^{-7}–10^{-8} W) have been obainted as 6th harmonic from 64.2 GHz and as 5th harmonic from 100 GHz, respectively. The performance of the harmonic generators is discussed in more details in Sect. 2.5 and compared with results obtained by other investigators.

2.2 THE SUPERHETERODYNE DETECTION SYSTEM

The harmonic mixer forms the frequency converter of the superheterodyne detection system. The intermediate frequency (IF) signal obtained from the harmonic mixer is the beat signal between the submillimeter signal and the n-th harmonic of the local oscillator (LO).

In the present experiments two different types of harmonic mixers were used. In the preliminary stages of the experiment (DIJ 68) harmonic mixers were used which mechanically were identical to the harmonic generator as shown in Fig. 2.1. The structure of these harmonic mixers is satisfactory for intermediate frequencies up to 250 MHz. In a superheterodyne detector the local oscillator

produces excess noise at the IF. This noise is the largest at the frequency of the LO signal and decreases with increasing frequency separation from the LO frequency. Consequently the LO noise problem may be circumvented by using a sufficiently high IF (WEN 64). Therefore a new harmonic mixer suitable for high IF signals has been designed. In the following the complete detection system with the harmonic mixers suitable for low and high IF will be described.

A Detection system with harmonic mixer for low IF

The harmonic mixer in this system is mechanically identical to the harmonic generator as given in Fig. 2.1. The mixer contains a tungsten whisker and a tellurium doped GaAs crystal, having a resistivity of about 0.003 ohm cm. The thickness of the crystal is 200 μm and it has been soldered with tin on a brass pen. A more detailed description of the harmonic mixer is given in the thesis of Huiszoon (HUI 66b). The mixer is driven by 60 GHz klystron (OKI, 60V10) and the IF is 100 MHz. The IF signal is applied through a matching section to a pre-amplifier (LEL, OMP-5080) which has a bandwidth from 80 to 160 MHz, 50 ohm input impedance, and a noise figure of 5.4 dB. The output of the pre-amplifier is applied to a tunable amplifier (Rohde & Schwarz, ASV) which also contains the second detector.

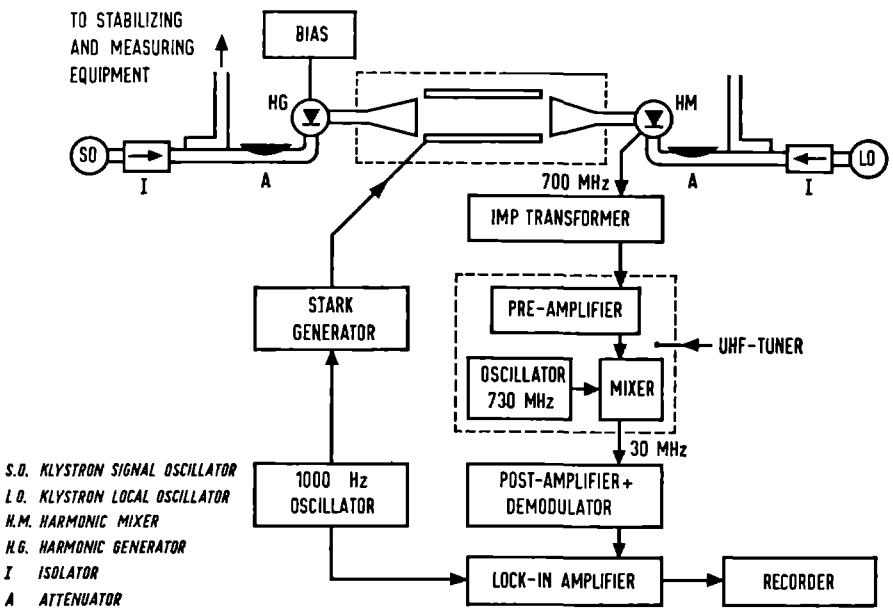

FIG. 2.3 Diagram of the absorption cell with horns and the superheterodyne detection system with phase sensitive demodulation.

B Detection system with harmonic mixer for high IF

The superheterodyne detection scheme for high IF signals is a part of the scheme, given in Fig. 2.3. This figure contains the harmonic generator with the driving (SO) klystron, the parallel-plate cell with horns, the superheterodyne detection system, the phase sensitive demodulation, and the recorder. The phase sensitive demodulation will be described at the end of this section. The superheterodyne mixing results in a signal at the IF usually of 700 MHz. For operation at this high frequency the construction of the IF output of the harmonic mixer has been modified as shown in Fig. 2.4. The harmonic mixer is described below. The IF signal is applied through an impedance transformer to an UHF-tuner (Philips). The tuner contains a pre-amplifier with noise figure of 10.8 dB, a mixer, and an oscillator. In the tuner the 700 MHz is converted into 30 MHz. The 30 MHz signal from the tuner is applied to a post-amplifier (AIL, 13240) which also contains the video detector. The bandwidth of the system is 4 MHz.

C Harmonic mixer for high IF

A cross-sectional view of the harmonic mixer for high IF is shown in Fig. 2.4. This mixer is a modification of the design of Cohn *et al* (COH 63) and of the harmonic mixer mentioned in Sect. 2.2A. The crystal is in the harmonic waveguide and the whisker protrudes through both waveguides. In addition the IF output has been improved to extract efficiently high IF frequencies.

The impedance of the GaAs diode is estimated to be 200 ohm at a LO power level of 20–40 mW (WEN 64). Therefore an IF impedance matching section, in which stepwise transitions from the 200 ohm impedance of the diode to a 50 ohm output-impedance are archieved, has been designed. An enlarged cross-sectional view of the diode and the IF output is given in Fig. 2.5. The capacitance C_1 between the thin end of the crystal pen and the wall of the hole in the secundary waveguide, and the capacitance C_2 between outer wall of secundary waveguide and crystal pen can be calculated from standard formulae, if edge effects are neglected. In this way the dimensions, which determine the capacitances C_1 and C_2, have been calculated. In order to obtain optimum conditions for the mixer, the final dimensions were determined by trial and error. For this purpose it was found useful to vary the capacitances C_1 and C_2 slightly: i) by modifying the length of the thin end of the crystal pen and the distance between the outer wall of the waveguide and the pen; ii) by placing a material with higher dielectric constant than air in the space of C_2. The impedance of the coaxial line consisting of crystal pen and holder was calculated also from a well known formula. The dielectric material in the coaxial line is

Rexolite with dielectric constant $\varepsilon = 2.72$ and magnetic permeability $\mu = 1$. For $b/a = 4.0$, where a is the diameter of the pen and b the inner diameter of the holder, the impedance equals about 50 ohm corresponding to the input impedance of the pre-amplifier.

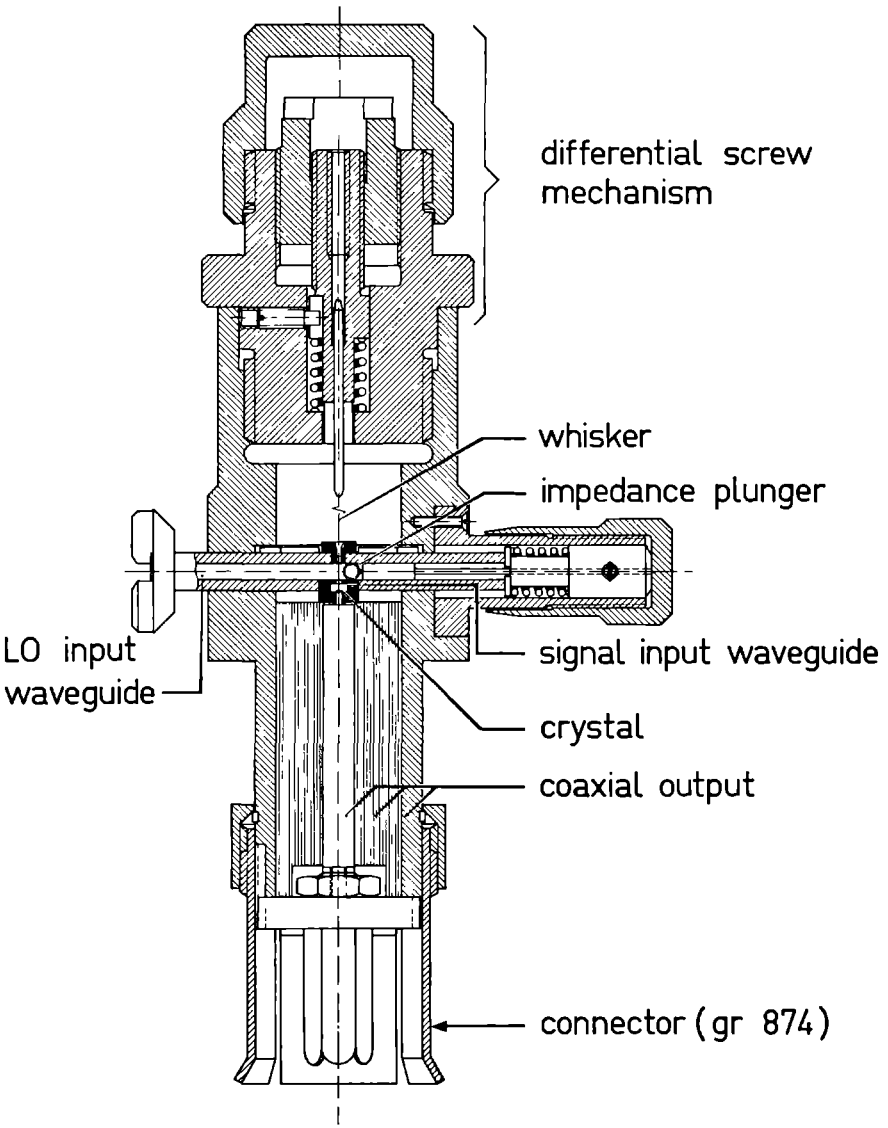

FIG. 2.4 Cross-sectional view of the harmonic mixer for high IF.

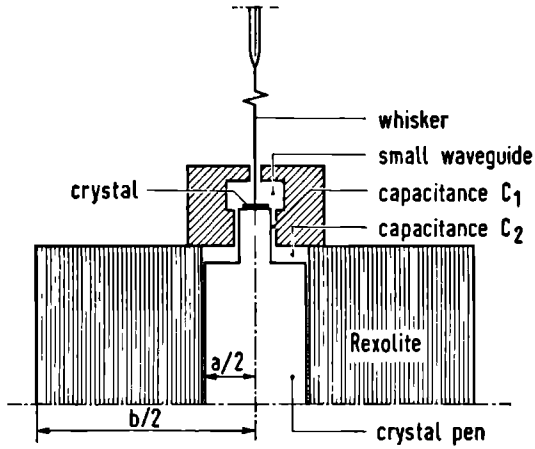

FIG. 2.5 Diode and IF output of harmonic mixer for high IF.

Two harmonic mixers of this design have been built, differing only in the dimensions of the input waveguides for the signal and the LO power. One mixer is driven by a 60 GHz klystron (OKI, 60V10) and has a LO input waveguide of 3.10 × 1.55 mm ID, and a signal input waveguide of 1.65 × 0.825 mm ID. The other mixer is driven by a 100 GHz klystron (Varian, VC735) and has a LO input waveguide of 2.54 × 1.27 mm ID, and signal input waveguide of 1.65 × 0.825 mm ID, which has been squeezed to 1.09 × 0.55 mm ID (compare with the harmonic generators in Sect. 2.1).

The harmonic mixer contains a small GaAs crystal 100 μm thick. The crystal has been soldered on a gold pen by heating the pen to about 550°C. The whisker is an AuCu alloy, consisting of 75 % Au and 25 % Cu (MCC 67). It is pointed by etching in a solution of 5 % NaCN and 5 % $K_4Fe(CN)_63H_2O$. The diode characteristic of the welded junction is the same as given by Huiszoon (HUI 66b) for the GaAs crystal with tungsten whisker.

D Phase sensitive demodulation

For both detection systems (low and high IF) a narrow noise bandwidth is required for maximum sensitivity. This is achieved by low frequency (1 kHz) square-wave Stark modulation and synchronous demodulation. The Stark voltage is applied between the plates of the absorption cell. The output of the second detector is fed to a lock-in amplifier (EMC) with variable integration time. The d.c. output of the lock-in amplifier is applied to a recorder (Fig. 2.3).

The circuit for stabilizing and measuring the frequency of the 64 GHz signal oscillator (SO) klystron is given in Fig. 2.6.

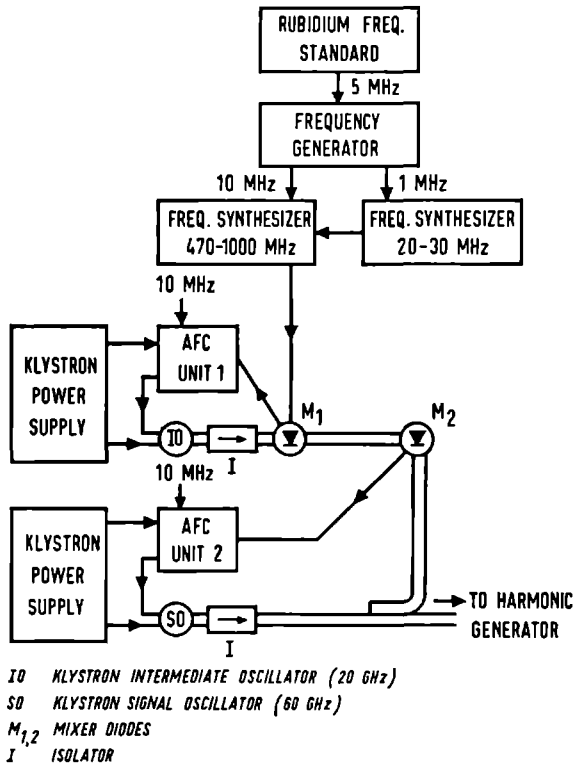

FIG. 2.6 Circuit for stabilizing and measuring the signal frequency.

The 5 MHz frequency signal from the rubidium frequency standard (Varian, R20) is applied to the external 'Control Steuerung' of the standard frequency generator (Rohde & Schwarz, XSU). From this a 10 MHz signal is applied to the 470–1000 MHz frequency synthesizer (Rohde & Schwarz, XUC) and a 1 MHz signal to the 20–30 MHz frequency synthesizer (Schomandl, ND30M). The output signal from the latter synthesizer is applied to the external 20–30 MHz input of the 470–1000 MHz synthesizer. The signal from the 470–1000 MHz synthesizer with frequency f_{st} is applied to the signal diode mixer M_1 (Schomandl, FMD 8/12). The rubidium standard is compared with 200 kHz frequency signal of station Droitwich.

The SO klystron can not be easily locked directly to the frequency standard because of its rather high (60–100 GHz) frequency. Therefore the SO klystron is locked to the standard through an intermediate oscillator (IO) klystron with lower (18–25 GHz) frequency than its own.

A fraction of the microwave signal from the IO klystron is applied simultaneously to the mixer M_1. The IO klystron (OKI, 20V10) has a frequency near 21.4 GHz. From the mixing process the resulting signal at the difference frequency near 30 MHz is applied to the automatic frequency control (AFC) unit 1 (Schomandl, FDS 30). The AFC unit has a reference input of 10 MHz, which comes from a standard frequency generator. The DC output signal of the AFC unit is applied to the reflector of the IO klystron. The frequency of the IO klystron is given by:

$$f_{IO} = (25f_{st} + 30)\ \text{MHz} \tag{2.1}$$

A fraction of the signal from the SO klystron is applied to the mixer diode M_2 through a directional coupler and mixed with the third harmonic of the signal from the IO klystron. From the mixing process a difference frequency near 30 MHz is obtained for the AFC unit 2 to synchronize the SO klystron. The frequency f_{SO} of the SO klystron follows then from

$$f_{SO} = (3f_{IO} + 30)\ \text{MHz} \tag{2.2}$$

The frequency f of the sixth harmonic of the SO klystron follows from Eqs. (2.1) and (2.2)

$$f = 6(3(25f_{st} + 30) + 30)\ \text{MHz} \tag{2.3}$$

For the LO klystron the frequency stabilizing and measuring set up is identical to that of the SO klystron, except for the 20–30 MHz frequency synthesizer which is not needed in the LO system. A practically identical system is used for the SO and LO klystrons at 100 GHz fundamental frequency.

For recording of the spectral lines the 10 MHz reference frequency signal for the AFC units is obtained from a frequency synthesizer (Schomandl, ND 5 and NDF 1). The frequency of this signal is varied by means of synchronous motor coupled to the axis of the fine tuning oscillator of the synthesizer.

2.4 THE SENSITIVITY OF THE SPECTROMETER

2.4.1 *The absorbed power in a molecular beam absorption cell*

The transition probability in molecular beam experiments is given by the Rabi-formula (RAM 56, p. 119; THA 61):

$$P_{ji} = \frac{|<j|\mu.E|i>|^2}{h^2(\nu_o - \nu)^2 + |<j|\mu.E|i>|^2} \times$$

$$\times \sin^2[(\nu_o - \nu)^2 + |<j|\mu.E|i>|^2/h^2]^{\frac{1}{2}} \pi t \qquad (2.4)$$

where P_{ji} gives the probability that a molecule originally in a state $|i>$ is found in a state $|j>$ after being subjected for a time t to an oscillating field $E\cos 2\pi\nu t$. It is assumed that $|i>$ and $|j>$ are isolated states with energies W_i and W_j. The resonance frequency ν_o equals $(W_j - W_i)/h$, where h is Planck's constant, and μ is the electric dipole moment.

We are interested in the case of resonance $\nu = \nu_o$ for the rotational transition $J \rightarrow J'$. The transition probability for absorption and stimulated emission has the same value. Therefore the power ΔP_{gas} absorbed by the gas molecules sent through the parallel-plate cell is given by the expression

$$\Delta P_{gas} = \sum_{MM'} h\nu_o n f_\nu (f_{JM} - f_{J'M'}) \sin^2 |<J'M'|\mu_E|JM>| \pi EL/h\nu \qquad (2.5)$$

where M is the quantum number of the component of J on the molecular axis, n is the number of molecules passing through the cell per second, f_ν is the fraction of the molecules in vibrational state v, f_{JM} is the fraction of the molecules in rotational state JM, L is the length of the molecular path in the cell (= width of the cell), v is velocity of the molecules, and μ_E is the component of the electric dipole moment along the direction of the microwave electric field **E**.

In Eq. (2.5) no allowance has been made for the nuclear spins. This will be done in Sect. 3.5 in the calculation of relative intensities.

For diatomic molecules the fraction f_{JM} in the rotational state JM with energy $W_J = hBJ(J+1)$ is given by the expression (TOW 55, p. 20)

$$f_{JM} = \frac{e^{-hBJ(J+1)/kT}}{\sum_{J=0}^{\infty} (2J+1)e^{-hBJ(J+1)/kT}} \qquad (2.6)$$

Here B is the rotational constant of the molecule, k is Boltzmann's constant, and T is the absolute temperature. If hB/kT is sufficiently small, the sum in Eq. (2.6) equals kT/hB and f_{JM} simplifies to:

$$f_{JM} = (hB/kT)e^{-hBJ(J+1)/kT} \qquad (2.7)$$

With this expression the absorbed power by the molecular beam becomes:

$$\Delta P_{gas} = nf_v e^{-hBJ(J+1)/kT} hB(h\nu_0/kT)^2 \times$$

$$\times \sum_{MM'} \sin^2 | < J'M' | \mu_E | JM > | \pi EL/h\nu \qquad (2.8)$$

For the microwave electric field along the z-axis, the dipole moment matrix elements in Eq. (2.8) are different from zero only for $J' = J \pm 1$ and $M' = M$ (TOW 55, p. 22):

$$< J+1M | \mu_z | JM > = \mu \left(\frac{(J+1)^2 - M^2}{(2J+1)(2J+3)} \right)^{\frac{1}{2}}$$

$$< J-1M | \mu_z | JM > = \mu \left(\frac{J^2 - M^2}{(2J-1)(2J+1)} \right)^{\frac{1}{2}} \qquad (2.9)$$

In an actual beam the molecules have a Maxwellian beam velocity distribution. The averaging over this distribution gives for the transition probability for beam absorption (RAM 56, p. 123):

$$< \sin^2 < J'M | \mu_z | JM > \pi EL/h\nu >_{Av} = \tfrac{1}{2} - I(2\pi < J'M | \mu_z | JM > EL/h\alpha) \qquad (2.10)$$

where $\alpha = (2kT/m)^{\frac{1}{2}}$ is the most probable velocity, and m is the molecular mass. The function I (x) has been defined and tabulated in the book of Ramsey (RAM 55, p. 425).

2.4.2 *The power inducing maximum absorption and the maximum absorbed power in the rotational transition $J = 0 \rightarrow 1$*

From Eq. (2.10) follows that the transition probability is maximum if the function I (x) is minimum. The minimum value of I (x) = — 0.27 for x = 3.8. From this follows for the amplitude E_{max} which induces maximum absorption for the transition $JM \rightarrow J \pm 1M$,

$$E_{max} = \frac{1.9\, h\alpha}{< J \pm 1M | \mu_z | JM > \pi L} \qquad (2.11)$$

On the other hand for radiation with an electric field $E\cos 2\pi\nu t$, the energy density W of the electromagnetic field between the plates of the cell is given by:

$$W = \tfrac{1}{2} \varepsilon_0 E^2 \qquad (2.12)$$

where ε_0 is the permittivity of free space. The power P travelling through the cell is given by:

$$P - cdLW \tag{2.13}$$

where c is the velocity of light and d the separation between the plates. From Eqs. (2.11), (2.12) and (2.13) follows for the (sub)millimeter power P_{max} inducing maximum absorption:

$$P_{max} = 1.8 \frac{c\varepsilon_0 h^2 \alpha^2 d}{|\langle J + 1M | \mu_z | JM \rangle|^2 \pi^2 L} \tag{2.14}$$

The maximum absorbed power $(\Delta P_{gas})_{max}$ in the case of $JM \rightarrow J + 1M$ transition follows from Eqs. (2.8) and (2.10) with $I(x) = -0.27$

$$(\Delta P_{gas})_{max} = 0.77 n f_v c^{-hBJ(J+1)/kT} hB(h\nu_0/kT)^2 \tag{2.15}$$

In the case of $J \rightarrow J + 1$ transition the values of P_{max} and $(\Delta P_{gas})_{max}$ are more difficult to obtain. For this case the sum over M of the transition probabilities, averaged over the velocity distribution, must be calculated numerically as function of E. The value of E for which the sum is maximum, is E_{max}, from which the value of P_{max} follows. Substitution of the maximum value of the sum in Eq. (2.8) gives the value of $(\Delta P_{gas})_{max}$. However, in the particular case of the $J = 0 \rightarrow 1$ transition the results of Eqs. (2.14) and (2.15) are applicable.

The values of P_{max} and $(\Delta P_{gas})_{max}$ for the $J = 0 \rightarrow 1$ transition of the molecules HI, HBr and DBr are given in Table 2.1. At the temperature $T = 293°K$ nearly all molecules of these gases are in the ground vibrational state, so $f_v = 1$. The number n of molecules given in Table 2.1 represents the number of molecules passing through the parallel-plate cell per second. The pressure at

TABLE 2.1

molecule	frequency $J - 0 \rightarrow 1$ transition (GHz)	power inducing maximum absorption P_{max}(W)	number of molecules per second	maximum absorbed power $(\Delta P_{gas})_{max}$(W)
DBr^{79}	254	5.1×10^{-7}	2.3×10^{16}	2.6×10^{-9}
HI^{127}	385	1.1×10^{-6}	7.0×10^{16}	2.7×10^{-8}
HBr^{79}	500	5.1×10^{-7}	3.5×10^{16}	3.0×10^{-8}

the input of the effuser during the experiments has been chosen 36 mm Hg for HBr and HI, and 24 mm Hg for DBr. At these high pressures the directional function of the effuser-channels is lost. Therefore the number n is about 5×10^{-5} of the total number of molecules coming from the effuser (HUI 66b).

2.4.3 *The minimum detectable power*

Sensitivity of an apparatus for radiometry or spectroscopy can be given in terms of the minimum detectable power or the noise equivalent power (n.e.p.). The minimum detectable power P_{min} for superheterodyne detection is (MAR 67):

$$P_{min} = 2kTF(B_{IF}B_{out})^{\frac{1}{2}} \tag{2.16}$$

where B_{IF} the IF bandwidth and B_{out} the bandwidth of the final stage of the detector. With phase sensitive detection at an intermediate frequency we have $B_{IF} = B_{out}$. The discrepancy in performance between an ideal and a practical detector is expressed by the total noise factor F, given by:

$$F = L_M(F_{IF} + t - 1) \tag{2.17}$$

where L_M is the conversion loss of harmonic mixer, F_{IF} is the noise factor of the IF amplifier, and t is the crystal noise ratio, including contribution of the noise of the local oscillator. Eq. (2.16) is valid for root mean square noise.

In absorption spectroscopy small variations in the radiation power P are to be observed. Sensitivity of a spectrometer is then determined by the minimum detectable absorbed power ΔP_{min}. For superheterodyne detector with phase sensitive detection the power ΔP_{min} is given by Huiszoon (HUI 66b)

$$\Delta P_{min} = \pi(2kTFB_0P)^{\frac{1}{2}} \tag{2.18}$$

where the bandwidth B_0 equals the reciprocal of the integration time of the phase sensitive detector.

It is possible to determine if sufficient power is available to induce maximum absorption by observing the output signal as a function of the input power. The experiments have shown that this is not the case for the rotational transition $J = 0 \rightarrow 1$ of HBr, DBr and HI. Consequently the following procedure was developed to determine P_{min}.

We consider the $J = 0 \rightarrow 1$ transition of HBr at 500 GHz and assume a certain value for the submillimeter power P. From Eqs. (2.12) and (2.13) we get

then the value of electric field E and subsequently the transition probability from Eq. (2.10). Substitution of this transition probability into Eq. (2.8) gives the value of ΔP_{gas} at the assumed value of P. In Table 2.2 the values of ΔP_{gas} are given as function of the value of P, starting with the value of P_{max}. The sum of the signal to noise ratios of all hyperfine components of the rotational transition of HBr gives a value of 540 for the signal to noise ratio of the line. Assuming ΔP_{min} equals $\Delta P_{gas}/540$ at all values of $P < P_{max}$, then the value of the total noise factor F is obtained from Eq. (2.18) with $B_o = 1$ Hz and $kT = 4 \times 10^{-21}$ W at the various submillimeter powers (Table 2.2). The highest value of F from Table 2.2 is then accepted as the value of F at 500 GHz. It should be emphasized that the actual value of F is properly lower than this upper limit of F. With this value for F the n.e.p. is obtained from Eq. (2.16) for bandwidths $B_{IF} = B_{out} = 1$ Hz. The result is given in Table 2.3.

The same procedure was followed for the 385 GHz and 254 GHz rotational transition $J = 0 \rightarrow 1$ of HI and DBr, respectively. The signal to noise ratios are 540 and 270 for HI and DBr, respectively. The results for the total noise factor and the n.e.p. are also given in Table 2.3.

TABLE 2.2 Determination of the upper limit for the total noise factor at the 500 GHz from the rotational transition of HBr.

submillimeter power (W)	absorbed power ΔP_{gas} (W)	total noise factor F
5.10×10^{-7}	3.00×10^{-8}	7.8×10^{4}
2.55×10^{-7}	2.64×10^{-8}	11.3×10^{4}
1.70×10^{-7}	2.25×10^{-8}	12.9×10^{4}
1.28×10^{-7}	1.92×10^{-8}	12.5×10^{4}
1.02×10^{-7}	1.67×10^{-8}	12.0×10^{4}
5.6×10^{-8}	1.1×10^{-8}	10×10^{4}
2.0×10^{-8}	0.5×10^{-8}	5×10^{4}
1.3×10^{-9}	0.04×10^{-8}	0.4×10^{4}

TABLE 2.3 The noise equivalent power at different frequencies as obtained in the present experiments.

frequency (GHz)	harmonic number of mixing	total noise factor	n.e.p. (W) $B_{IF} = B_{out} = 1$ Hz
254	4	4.0×10^{3}	3×10^{-17}
385	6	4.9×10^{4}	4×10^{-16}
500	5	12.9×10^{4}	1×10^{-15}

2.5.1 *Comparison with other submillimeter detectors*

Detectors for millimeter, submillimeter and far infrared may be classified into three groups according to the physical process responsible for their operation. These are the thermal, the photoconductive, and the semiconductor junction detectors. Reviews of the performance of these detectors, video as well as fundamental and harmonic mixers, are given among others by Martin (MAR 67) and by Kneubühl (KNE 69). A short summary of representative data of these detectors as mixers with or without phase sensitive demodulation is given in Table 2.4. In order to compare correctly all results in Table 2.4, the values of the n.e.p. for superheterodyne detectors without modulation have

TABLE 2.4

frequency or wavelength range	method – superheterodyne detector – video detector	IF bandwidth or modulation	n.e.p. (W) for 1 Hz bandwidth	reference
140 GHz	Ge point-contact fund. mixing	B_{IF} – 60 MHz	1×10^{-18}	(MER 63)
254 GHz	GaAs point-contact 4th harm. mixing	modulation of absorbed signal	3×10^{-17}	present work
385 GHz	GaAs point-contact 6th harm. mixing	modulation of absorbed signal	4×10^{-16}	present work
500 GHz	GaAs point-contact 5th harm. mixing	modulation of absorbed signal	1×10^{-15}	present work
600 GHz	GaAs point-contact 2th harm. mixing	$B_{IF} = 1.6$ GHz	1×10^{-17}	(BAU 66)
890 GHz	Ge point-contact fund. mixing	$B_{IF} = 1$ MHz	1×10^{-16}	(PAY 70)
100 GHz	Ge point-contact video	modulation of signal	5×10^{-11}	(BEC 70)
1000 GHz	Ge point-contact video	modulation of signal	2×10^{-8}	(BEC 70)
near infrared to several mm	He-cooled (2.1 K) Ge bolometer	modulation of signal	3×10^{-12}	(MAR 67)
far infrared	^{3}He-cooled (0.37 K) Ge bolometer	modulation of signal	3×10^{-14}	(DRE 69)
600 GHz (1 mm to 100 μm)	He-cooled (1.5 K) InSb photoconductive detector	modulation of signal	1×10^{-11}	(PUT 65)

been given for $B_{IF} = 1$ Hz. The experimental results in the relevant cases are the following: 1) Meredith and Warner (MER 63) give n.e.p. of 7×10^{-15} W at an IF bandwidth of 60 MHz, corresponding with a total noise factor of 20 dB; 2) Bauer *et al* (BAU 66) give a total noise factor of about 30 dB at an IF bandwidth of 1.6 GHz; 3) Payne and Prewer (PAY 70) give n.e.p. of 10^{-13} W at an IF bandwidth of 1 MHz.

The point-contact mixers are very sensitive detectors in comparison with the point-contact video detectors, but also in comparison with He-cooled bolometers and photoconductive detectors. However, the sensitivity of the point-contact mixers decreases with increasing frequency and with the order of the harmonic mixing. Klystrons with frequencies higher than 100 GHz are very expensive in view of their short live. The results of Bauer et al obtained with a carcinotron as LO and of Payne and Prewer obtained with a laser as LO are not very interesting for spectroscopy because of the very narrow frequency region covered by these mixers. On the other hand bolometers are suitable for a great frequency region. Furthermore, the results for the harmonic mixers in the present work were obtained with modulation of only the absorbed power, while the results for the bolometers were obtained with modulation of the total power. Modulation of the total power that is incident on the detector will result in low frequency noise being converted to modulation frequency because of the mixing properties of the detector (MAR 67). Consequently, for spectroscopy in the frequency region of 500–700 GHz we can not conclude if the point-contact mixers are superior to the ^{3}He-cooled bolometer or vice versa. This depends strongly on the order of the harmonic mixing. From about 700 GHz the ^{3}He-cooled bolometer will most probably be superior to the point-contact harmonic mixers at increasing frequencies.

2.5.2 *Performance of superheterodyne detection systems A and B*

The performance of superheterodyne detectors is determined by the total noise factor. This factor is determined by the conversion loss of the harmonic mixer, the noise factor of the intermediate frequency amplifier and the crystal noise ratio (including contribution of the local oscillator noise).

The detector A with harmonic mixer for low IF has a rather high value for the crystal noise ratio. Huiszoon (HUI 66b, p. 49) gives for this detector at IF between 100–200 MHz a crystal noise ratio of 23 (160 GHz, 4th harmonic) and 55 (215 GHz, 3th harmonic). Values given by Huiszoon for the conversion loss of the harmonic mixer are given in Table 2.5.

The detector B with harmonic mixer for high IF has a low value for the crystal noise ratio. According to Cotton (COT 63) the crystal noise ratio at IF of

700 MHz can be as low as two for higher harmonic mixing. With values of the total noise factor from Table 2.3 and a value of 10.8 dB for the noise factor of the IF amplifier we obtain from Eq. (2.17) values for the conversion loss of the harmonic mixers given in Table 2.5. Bauer *et al* (BAU 66) have obtained values for the conversion loss of the harmonic mixers as a function of the frequency for second and third harmonic order. An extrapolation of Bauer's results suggests an increase in conversion loss of roughly 4 dB per harmonic starting from the second harmonic. These values are also given in Table 2.5.

TABLE 2.5 Conversion loss of harmonic mixers.

reference	frequency (GHz)	harmonic number	conversion loss (dB)	remark
Huiszoon	160	4	28	n-doped GaAs
	216	3	26	(200 μm thick)
				tungsten whisker
present	254	4	25	n-doped GaAs
investigation	385	6	36	(100 μm thick)
	500	5	40	gold-copper whisker
Bauer	160	4	21	n-doped GaAs
	216	3	19	(a wafer)
	254	4	24	phosphor-bronze
	385	6	35	whisker
	500	5	33	

The correspondence between Bauer's results and the present investigation is very good for the 4th and 6th harmonic of 64 GHz. The discrepancy for the 5th harmonic of 100 GHz can be explained by a too high value for the total noise factor (Sect. 2.4.3). The upper limit of the total noise factor has been calculated for a power of about 2×10^{-7} W from the harmonic generator. If the power is rougly 10 times smaller, then the total noise factor becomes 5.0×10^4 and the conversion loss 36 dB.

2.5.3 *Performance of the harmonic generators*

No exact values of the powers from the harmonic generators used in the present experiments can be given. The values are lower than the values in Table 2.1 for the powers inducing maximum absorption, P_{max}. From the agreement between the conversion loss factors obtained in the present experiments and those of Bauer we estimate that the power of the harmonic gene-

rator at 385 GHz and 255 GHz is of the order of 3×10^{-7} W. The relatively poor result for 255 GHz can be explained from the fact that no efforts have been done to improve the results and by deterioration of the Ohl-crystals used intensively during two years. Estimated power for the 5th harmonic of 100 GHz is about 2×10^{-8} W. At input powers of 100–200 mW these submillimeter powers give rather high values for the conversion loss of the harmonic generators.

Bauer *et al* (Bau 66) give values of harmonic generation conversion loss at various frequencies for several harmonic orders. Extrapolation of their results gives for the 6th harmonic at 385 GHz and the 5th harmonic at 500 GHz harmonic generation conversion loss factors of 43 dB and 40 dB, respectively, for fundamental signal powers of 10–20 mW.

From the harmonic generator driven by a 100 GHz klystron we have obtained also 600 GHz and 700 GHz signals. The signal at 600 GHz was $5\times$ and the signal at 700 GHz $20\times$ smaller than the 500 GHz signal. The detection has been done with the harmonic mixer also driven by a 100 GHz klystron. The method to detect these signals on the scope is described by Overbeek (OVE 68). A filter with cut-off frequency of about 335 GHz has been placed between harmonic generator and harmonic mixer. This was done to make sure that the harmonic mixer output for all SO harmonics with frequencies from 400 GHz to 800 GHz is a reliable indication of the presence of these harmonics. Spurious signals due to IF-mixing are then completely eliminated (OVE 68). So far no molecular beam spectroscopy has been done with these signals.

The conclusion is that some improvement in the generation of submillimeter power with point-contact harmonic generators will lead to submillimeter powers useful also for molecular beam spectroscopy at frequencies up to at least 800 GHz.

CHAPTER 3

THEORY

3 1 ROTATION-VIBRATION ENERGIES

From experimental studies of molecular spectra and from ab initio calculations on simple molecules it is known that an adequate rotation-vibration potential function for diatomic molecules is given by the Dunham potential (TOW 55, p. 10; HER 50, p. 107):

$$V(R) = a_0\zeta^2(1 + a_1\zeta + a_2\zeta^2 + \ldots) + B_eJ(J + 1)(1 - 2\zeta + 3\zeta^2 - \ldots) \quad (3.1)$$

The approximate rotation-vibration energies W_{Jv} obtained with this potential are given by:

$$W_{Jv}/h = \omega_e(v + \tfrac{1}{2}) - \omega_e x_e(v - \tfrac{1}{2})^2 + \ldots B_vJ(J + 1) - D_vJ^2(J + 1)^2 + \ldots \quad (3.2)$$

In the expressions (3 1) and (3.2) $\zeta = (R - R_e)/R_e$, where R_e is the equilibrium internuclear distance and R is the instantaneous distance of the two nuclei; a_i's are the Dunham potential constants, J is the rotational quantum number, v is the vibrational quantum number, ω_e is the fundamental vibrational frequency, $\omega_e x_e$ is a small constant depending on the anharmonicity of the potential function; B_v is the rotational constant in the $|\, v >$ vibrational state of the molecule defined by:

$$B_v = B_e - \alpha_e(v + \tfrac{1}{2}) + \gamma_e(v - \tfrac{1}{2})^2 + \ldots, \quad (3.3a)$$

where $B_e = h/8\pi^2\mu R_e^2$

is the rotational constant at the distance R_e, μ is the reduced mass of the molecule, and α_e and γ_e are small constants which measure the interaction between vibration and rotation. The centrifugal stretching constant D_v and D_e for the vibrational state $|\, v >$ and for the equilibrium distance, respectively, is defined by:

$$D_v = D_e + \beta_e(v - \tfrac{1}{2}) + \ldots$$
$$D_e = 4B_e^3/\omega_e^2 \quad (3.3b)$$

where β_e is a small constant.

The expressions (3.1) and (3.2) are derived using the Born-Oppenheimer approximation. Also contributions of hyperfine interactions and external fields are neglected for the moment. Furthermore we restrict ourselves to $^1\Sigma$ molecules. The frequency of a rotational transition $J \rightarrow J'$ in a given vibrational state follows from Eq. (3.2) and the selection rules $\Delta v = 0$ and $\Delta J = 1$.

3.2 HAMILTONIAN FOR HYPERFINE INTERACTIONS AND EXTERNAL ELECTRIC FIELD

The Hamiltonian for interpretation of the hyperfine structure and Stark effect in the rotational spectra of $^1\Sigma$ molecules has been investigated by Townes and Schawlow (TOW 55), Ramsey (RAM 56), Thaddeus *et al* (THA 64), Hirschfelder *et al* (HIR 65), Dymanus (DYM 66), Verhoeven (VER 69), and by others. These investigations have shown that the following Hamiltonian (VER 69) is fully adequate for the interpretation of spectra observed in the present investigation:

$$\mathbf{H} = \sum_K \mathbf{Q}_K : \mathbf{V}_K + \sum_K \sum_{L>K} \mathbf{I}_K.\mathbf{D}_{KL}.\mathbf{I}_L + \sum_K \mathbf{I}_K.\mathbf{M}_K.\mathbf{J} - \mu.\mathbf{E} - \tfrac{1}{2}\mathbf{E}.\alpha.\mathbf{E} \qquad (3.4)$$

Herein, and in the following, the capital subscripts K, L refer to nuclei and the subscripts i, j to electrons; $\mathbf{I}_K$ is the nuclear spin of the K-th nucleus, and $\mathbf{J}$ is the rotational angular momentum.

The first term of Eq. (3.4) represents the interaction of the electric quadrupole moment of the K-th nucleus with the gradient of the electric field because of the surrounding electronic and nuclear charges. Expressions for the nuclear quadrupole tensor $\mathbf{Q}_K$ and the tensor $\mathbf{V}_K$ of the molecular electric field gradient can be found elsewhere (VER 69; RAM 56).

The second term is the nuclear spin-spin interaction. In principle, the spin-spin interaction contains the direct, or nuclear spin-spin, interaction between two nuclear magnetic dipole moments, and the indirect, or electron coupled, spin-spin interaction. The energy of the electron coupled spin-spin interaction (RAM 56) is below the resolving power of the present beam-spectrometer. Consequently the spin-spin term in the Hamiltonian contains only the direct interaction, expressed with the aid of the molecular coupling tensor $\mathbf{D}_{KL}$, of which the components are given in Table 3.1. Herein $\mathbf{r}_{pq} = \mathbf{r}_p - \mathbf{r}_q$ and $r_{pq} = |\mathbf{r}_{pq}|$, where $\mathbf{r}_q$ is the position vector of q-th particle with respect to the molecular center of mass; μ_N is the nuclear magneton, g_K is the nuclear g factor of nucleus K, and μ_o is the permeability of the free space.

The third term is the spin-rotation interaction. The molecular coupling tensor tensor for nucleus K contains a nuclear and electronic part: $\mathbf{M}_K = \mathbf{M}_K^{(n)} +$

TABLE 3.1 Expressions for the components of the molecular electric dipole moment μ, and the molecular coupling tensors $M_K^{(n)}$, $M_K^{(e)}$, D_{KL}, and α, all referred to the principal axes g = a, b, c of a molecule.

$$(D_{KL})_{gg'} = (\mu_o/4\pi)\mu_N^2 g_K g_L r_{KL}^{-5}[r_{KL}^2\,\delta(g, g') - 3(r_{KL})_g(r_{KL})_{g'}]$$

$$(M_K^{(n)})_{gg'} = -2c(\mu_o/4\pi)\mu_N g_K A_g \sum_{L\neq K} Z_L r_{KL}^{-3}[r_{KL}^2\,\delta(g, g') - (r_{KL})_g\,(r_{KL})_{g'}]$$

$$(M_K^{(e)})_{gg'} = -2e(\mu_o/4\pi m)\mu_N g_K A_g \sum_{n\neq o} [(E_o - E_n)^{-1} <o \mid \sum_i (r_{iK} \times$$

$$\times (p_i - p_K))_g r_{iK}^{-3} \mid n> <n \mid \sum_i (r_{iK} \times (p_i - p_K))_{g'} \mid o> + \text{c.c.}]$$

$$\alpha_{gg'} = -e^2 \sum_{n\neq o} (E_o - E_n)^{-1}[<o \mid \sum_i (r_i)_g \mid n><n \mid \sum_i (r_i)_{g'} \mid o> + \text{c.c.}]$$

$$\mu_g = e\sum_K Z_K(r_K)_g - e\sum_i <o \mid (r_i)_g \mid o>$$

$M_K^{(e)}$. The components of these coupling tensors are given in Table 3.1. Herein $A_g = 1/2I_g$ is the rotational constant with I_g as the moment of inertia about the g-axis, where g = a, b, c stands for one of the principal axes; eZ_q and $\mathbf{p}_q$ is the charge and momentum of particle q, respectively; m is the electronic mass, $\mid n>$ represents the electronic state and E_n its corresponding eigen value, under assumption of the Born-Oppenheimer approximation.

The fourth and fifth term represent the interaction of the permanent electric dipole moment μ and of the induced electric dipole moment $\alpha.\mathbf{E}$, respectively, with the external electric field $\mathbf{E}$. Expressions for the components of μ and of the molecular polarizability tensor α are also given in Table 3.1.

The Hamiltonian is derived using the rigid rotor approximation. The effect of vibrations on the expectation values of the various contributions to the Hamiltonian will be treated in Sect. 5.1. as perturbation.

3.3 MATRIX ELEMENTS OF THE HYPERFINE HAMILTONIAN FOR HI, HBr AND DBr

The energies of the hyperfine sublevels of a given rotational J-level are obtained as solutions of the secular equation of the Hamiltonian (3.4). In the absence of external fields (E = o) the most appropriate representation is:

$$\mid (JI_1)F_1I_2FM_F>, \text{ abbreviated as } \mid F_1FM_F>,$$

with the coupling scheme:

$$\mathbf{J} + \mathbf{I}_1 = \mathbf{F}_1 \quad \text{and} \quad \mathbf{F}_1 + \mathbf{I}_2 = \mathbf{F},$$

where the subscript 1 of the nuclear spin vector denotes the halide nucleus ^{127}I (spin 5/2) or ^{79}Br, ^{81}Br (spin 3/2), and the subscript 2 denotes the hydrogen nucleus ^{1}H (spin 1/2) or ^{2}H (spin 1); M_F is the projection of **F** on the space fixed z-axis.

After the terms in the Hamiltonian have been expressed in spherical tensor operators, the matrix elements of the hyperfine interactions can be calculated in the chosen representation with the aid of tensor operator techniques (JUD 63, Chap. 3).

a Spin-rotation interactions

The spin-rotation term of Eq. (3.4) for nucleus 2 can be expressed in spherical tensors (HUI 66b):

$$\mathbf{I}_2.\mathbf{M}_2.\mathbf{J} = \sum_{k=0,1,2} (-)^k (2k+1)^{\frac{1}{2}} \{(I_2)^{(1)} \{(M_2)^{(k)} J^{(1)}\}^{(1)}\}^{(0)} \tag{3.5}$$

The spherical components in terms of the Cartesian components are given in the cited reference.

Using tensor operator techniques the matrix elements of $\mathbf{I}_2.\mathbf{M}_2.\mathbf{J}$ can be evaluated in the $| F_1 F M_F >$ representation as:

$$< F_1 F M_F \,|\, \mathbf{I}_2.\mathbf{M}_2.\mathbf{J} \,|\, F_1\, 'F' M_F' > =$$

$$= \delta(F,F')\,\delta(M_F,M_F')\,(-)^{J+I_1+I_2+2F_1'+F+1}\,[(2F_1+1)(2F_1'+1)]^{\frac{1}{2}} \times$$

$$\times \begin{Bmatrix} F & I_2 & F_1' \\ I & F_1 & I_2 \end{Bmatrix} \begin{Bmatrix} I_1 & J & F_1' \\ I & F_1 & J \end{Bmatrix} < I_2 \| (I_2)^{(1)} \| I_2 > < J \| J^{(1)} \| J > \times$$

$$\times \sum_k (-)^k (2k+1)^{\frac{1}{2}} \begin{Bmatrix} k & I & I \\ J & J & J \end{Bmatrix} < J \| (M_2)^{(k)} \| J > \tag{3.6}$$

The reduced matrix elements of Eq. (3.6) can be evaluated with the aid of the Wigner-Eckart theorem. The components of the interaction tensor $M^{(k)}$ are written in terms of molecular constants by transforming these components from the space-fixed to the molecule-fixed CM system (EDM 60, p. 71). The resulting relations for the reduced matrix elements of the interaction tensor are (HUI 66b, LEE 67):

$$< J \| M^{(0)} \| J > = -\begin{bmatrix} 2J+1 \\ 3 \end{bmatrix}^{\frac{1}{2}} (M_{aa} + M_{bb} - M_{cc})$$

$$< J \| M^{(1)} \| J > = 0 \tag{3.7}$$

$$< J \| M^{(2)} \| J > = \begin{bmatrix} (2J+2)(2J+1)(2J) \\ 24(2J+3)(2J-1) \end{bmatrix}^{\frac{1}{2}} (M_{aa} + M_{bb} - 2M_{cc})$$

By substituting these relations in Eq. (3.6) and evaluating the 6-j symbol in the sum over k, we obtain the matrix elements in terms of 6-j symbols (ROT 59) and a coupling constant:

$$< F_1 F M_F \mid \mathbf{I}_2.\mathbf{M}_2.\mathbf{J} \mid F_1' F' M_F' > =$$

$$= \delta(F,F')\,\delta(M_F,M_F')\,(-)^{J+I_1+I_2+2F_1'+F+1}\,[(2F_1'+1)(2F_1+1)I_2 \times$$

$$\times (I_2+1)(2I_2+1)J(J-1)(2J+1)]^{\frac{1}{2}} \begin{Bmatrix} F & I_2 & F_1' \\ I & F_1 & I_2 \end{Bmatrix} \begin{Bmatrix} I_1 & J & F_1' \\ I & F_1 & J \end{Bmatrix} C_2$$

where $C_2 = (M_2)_{aa} = (M_2)_{bb}$ (3.8)

In this way we obtain also the matrix elements of the spin-rotation term $\mathbf{I}_1.\mathbf{M}_1.\mathbf{J}$, which turns out to be diagonal in F_1. Consequently 6-j symbols in the expression for the matrix elements can be evaluated.
The result is:

$$< F_1 F M_F \mid \mathbf{I}_1 . \mathbf{M}_1.\mathbf{J} \mid F_1' F' M_F' > =$$

$$= \delta(F_1,F_1')\,\delta(F,F')\,\delta(M_F,M_F')\tfrac{1}{2}\,[F_1(F_1+1) - I_1(I_1+1) - J(J+1)]\,C_1$$

where $C_1 = (M_1)_{aa} = (M_1)_{bb}$ (3.9)

Generally, C_K in the expression (3.8) and (3.9) is the spin-rotation coupling constant of the K-th nucleus.

b Spin-spin interaction

The matrix elements of the spin-spin term are obtained in the same way:

$$< F_1 F M_F \mid \mathbf{I}_1.\mathbf{D}.\mathbf{I}_2 \mid F_1' F' M_F' > = \delta(F,F')\,\delta(M_F,M_F')\,(-)^{F_1'+I_2+F+1} \times$$

$$\times (15/2)^{\frac{1}{2}}[(2F_1'+1)(2F_1+1)I_1(I_1+1)(2I_1+1)I_2(I_2+1)(2I_2+1)]^{\frac{1}{2}} \times$$

$$\times \begin{Bmatrix} F & I_2 & F_1' \\ I & F_1 & I_2 \end{Bmatrix} \begin{Bmatrix} J & J & 2 \\ I_1 & I_1 & I \\ F_1 & F_1' & I \end{Bmatrix} \begin{bmatrix} (2J+2)(2J+1)(2J) \\ (2J+3)(2J-1) \end{bmatrix}^{\frac{1}{2}} d_T, \tag{3.10}$$

where $d_T = (\mu_0/4\pi)\mu_N^2 g_1 g_2 r_{12}^{-3}$

is the nuclear spin-spin coupling constant of the nuclei 1 and 2 of the molecule. In the derivation of Eq. (3.10) use has been made of the relation $\Sigma_g D_{gg} = 0$, which follows from the definition of $D_{gg'}$, as given in Table 3.1. The 9-j symbol can be written as a sum over 6-j symbols (JUD 63; EDM 60). For the diagonal elements the 9-j symbol of Eq. (3.10) can be evaluated with the aid of an expression given by Edmonds (EDM 60, p. 119).

c Quadrupole interactions

By an analoque treatment, the matrix elements of the quadrupole interaction term are obtained (THA 64; DIJ 67):

$$< F_1 F M_F \mid \mathbf{V}_1 : \mathbf{Q}_1 \mid F_1' F' M_F' > = - \delta(F_1', F_1)\, \delta(F', F)\, \delta(M_F', M_F) \times$$

$$\times \left[\frac{(3/4)\, X(X+1) - I_1(I_1+1)\, J(J+1)}{2I_1(2I_1-1)\,(2J-1)\,(2J+3)} \right] (eqQ)_1 \qquad (3.11)$$

where $X = F_1(F_1+1) - J(J+1) - I_1(I_1+1)$

and $< F_1 F M_F \mid \mathbf{V}_2 : \mathbf{Q}_2 \mid F_1' F' M_F' > = \delta(F', F)\, \delta(M_F', M_F) \times$

$$\times (-)^{J+I_1+I_2+2F_1'+F+1} \begin{Bmatrix} I_1 & J & F_1' \\ 2 & F_1 & J \end{Bmatrix} \begin{Bmatrix} F & I_2 & F_1' \\ 2 & F_1 & I_2 \end{Bmatrix} \times$$

$$\times \left[\frac{(2F_1'+1)(2F_1+1)(2I_2+1)(2I_2+2)(2I_2+3)\, J\,(2J+1)(2J+2)}{8I_2(2I_2-1)\, 8(2J-1)\,(2J+3)} \right]^{\frac{1}{2}} (eqQ)_2 \qquad (3.12)$$

where $(eqQ)_K$ is the quadrupole coupling constant of the K-th nucleus with $q_K = (V_K)_{cc}$ as the c-component of the electric field gradient tensor at the K-th nucleus, and Q_K as the quadrupole moment of the K-th nucleus.

The only off-diagonal matrix elements for $J' \neq J$, which are of importance, are terms due to the quadrupole interaction of the halide nucleus. Expressions for these terms are given by Townes (TOW 55, p. 157). For a diatomic molecule only matrix elements with $J' = J \pm 2$ contribute to the energy.

3.4 MATRIX ELEMENTS OF THE STARK HAMILTONIAN FOR HI, HBr AND DBr

For a diatomic molecule the first order Stark effect is zero. The second order Stark effect is of the order of 0.1 MHz/(kV/cm)^2 for the molecules HI, HBr and

DBr. The applied electric fields are between 2–4 kV/cm. The quadrupole interaction of the halide nucleus gives splittings of the rotational levels of the order of 100 MHz, and the spin-rotation and spin-spin interactions give splittings of the order of 50 kHz. Therefore the most appropriate representation for the calculation of Stark splittings is the partly coupled representation:

$$| (JI_1)F_1I_2M_1M_2 >, \text{ abbreviated as } | JF_1M_1M_2 >,$$

with the coupling scheme:

$$\mathbf{J} + \mathbf{I}_1 = \mathbf{F}_1,$$

where M_1 and M_2 is the projection of $\mathbf{F}_1$ and $\mathbf{I}_2$ on the space fixed z-axis, respectively.

The matrix elements of the hyperfine Hamiltonian can be evaluated in the $| JF_1M_1M_2 >$ representation with the aid of 3-j symbols (ROT 59) and the expressions for the matrix elements in the $| F_1FM_F >$ representation as given in the foregoing section. In the first instance we have calculated the matrix elements of the hyperfine Hamiltonian in the fully coupled representation, because this representation is the most appropiate representation at zero Stark field. At this field we have done all initial experiments in order to obtain the hyperfine coupling constants (DIJ 68, DIJ 69).

a The interaction $-\mu.\mathbf{E}$

The matrix elements of the $\mu.\mathbf{E}$ interaction can be evaluated with the aid of the tensor operator techniques. The result is (OVE 68a):

$$< JF_1M_1M_2 | -\mu.\mathbf{E} | J'F_1'M_1'M_2' > = 0$$

for all values of J', except for $J' = J \pm 1$; and

$$< JF_1M_1M_2 | -\mu.\mathbf{E} | (J+1)F_1'M_1'M_2' > = \delta(M_1,M_1')\,\delta(M_2,M_2') \times$$

$$\times (-)^{J+I_1+F_1+F_1'-M_1+1}\,[(J+1)(2F_1+1)(2F_1'+1)]^{\frac{1}{2}} \times$$

$$\times \begin{pmatrix} F_1 & 1 & F_1' \\ -M_1 & 0 & M_1 \end{pmatrix} \begin{Bmatrix} I_1 & J+1 & F_1' \\ 1 & F_1 & J \end{Bmatrix} \mu E \qquad (3.15)$$

Because the matrix is symmetric, only the expression for the element with $J' = J + 1$ is given.

b The interaction $-\frac{1}{2}\mathbf{E}.\alpha.\mathbf{E}$

The matrix elements of the polarizability interaction can be evaluated in the same way as of the spin-rotation interaction. The expression for the matrix element diagonal in F_1 is (DIJ 70):

$$< JF_1M_1M_2 \mid -\tfrac{1}{2}\mathbf{E}.\alpha.\mathbf{E} \mid JF_1M_1'M_2' > = \delta(M_1,M_1')\,\delta(M_2,M_2') \times$$

$$\times \left[-\tfrac{1}{2}E^2\alpha_S - E^2\alpha_T \times \right.$$

$$\left. \times \frac{2[3M_1^2 - F_1(F_1+1)]\,[3Y(Y-1) - 4J(J+1)\,F_1(F_1+1)]}{(2F_1+3)\,(2F_1+2)\,(2F_1)\,(2F_1-1)\,(2J+3)\,(2J-1)} \right] \qquad (3.16)$$

where: $Y = J(J+1) + F_1(F_1+1) - I_1(I_1+1)$

and $\alpha_S = (1/3)\,(2\alpha_\perp + \alpha_{//})$

$\alpha_T = (1/3)\,(\alpha_\perp - \alpha_{//})$

where: $\alpha_\perp$ = polarizability perpendicular to bond direction,

$\alpha_{//}$ = polarizability along the bond direction.

Eq. (3.16) is only valid for $F_1 \neq \frac{1}{2}$. For $F_1 = \frac{1}{2}$ the coefficient of α_T is zero (property of a 6-j symbol). The scalar contribution of the polarizability is independent of the quantum numbers J and F_1 and it drops out of the expression for the transition frequencies. The matrix elements off-diagonal in F_1 may be neglected (DIJ 70).

3.5 CALCULATION OF THE RELATIVE INTENSITIES

In a beam spectrometer the intensity I_{if} of a transition from a initial state $\mid i >$ to a final state $\mid f >$ is proportional to (see Eqs. (2.4) and (2.8):

$$I_{if} \sim \sin^2 \mid < f \mid \mu.\mathbf{E} \mid i > \mid \pi L/h\nu \qquad (3.17)$$

where $\mathbf{E}$ is the microwave field strength. At sufficiently small E the intensity I_{if} becomes proportional to:

$$I_{if} \sim \mid < f \mid \mu_E \mid i > \mid^2 E^2 \qquad (3.18)$$

By writing the states $\mid i >$ and $\mid f >$ in terms of the unperturbed initial and final states $\mid g >$ and $\mid h >$, respectively,

$$| i > = \sum_g | g > R_{gi},$$

$$| f > = \sum_h | h > R_{hf},$$

the intensity matrix can be rewritten (in matrix notation) as:

$$\mathbf{I} = \mathbf{R}_f{}^{-} . \mathbf{C} . \mathbf{R}_i \tag{3.19}$$

Herein the elements C_{hg} of the matrix **C** are defined by:

$$C_{hg} = < h \mid \mu_E \mid g >,$$

and R_i and R_f are the unitary matrices which diagonalize the Stark and the hyperfine Hamiltonian of the initial and final state, respectively.

In the case of the Stark effect with hyperfine structure, the matrix elements C_{hg} are evaluated in the partly coupled representation and are given by Eq. (3.15).

In the case of the hyperfine structure without external field the matrix elements C_{hg} are evaluated in the fully coupled representation. Neglecting the above mentioned transformations **R** which give small corrections on the relative intensities, the relative intensities of the components of the rotational transition are after summation over the degenerate magnetic states:

$$| C_{JF_1F,J'F_1'F'} |^2 = \sum_{M_F,M_F'} | < JF_1FM_F \mid \mu_E \mid J'F_1'F'M_F' > |^2 =$$

$$= (1/3) | < JF_1F \| \mu^{(1)} \| J'F_1'F' > |^2 = (1/3)\,(2F + 1)\,(2F' + 1)\,(2F_1 + 1) \times$$

$$\times (2F_1' + 1) \begin{Bmatrix} F & F' & 1 \\ F_1' & F_1 & I_2 \end{Bmatrix}^2 \begin{Bmatrix} F_1 & F_1' & 1 \\ J' & J & I_1 \end{Bmatrix}^2 | < J \| \mu^{(1)} \| J' > |^2$$

For diatomic molecules, the reduced matrix element in Eq. (3.20) is zero for $\Delta J = 0$, and unequal zero for $\Delta J = \pm 1$. For the other values of J' the expression is zero because of the triangular conditions of the 6-j symbol. From the triangular relations of the 6-j symbols it follows also, that only $\Delta F_1 = 0$, ± 1 and $\Delta F = 0$, ± 1 transitions may occur.

EXPERIMENTAL RESULTS

4.1 HFS IN ROTATIONAL SPECTRA OF HI, HBr AND DBr[1]

4.1.1 *Calculation of the hyperfine coupling constants from the measured frequencies*

The frequencies of the hyperfine transitions are expressed in terms of the frequency ν_0 of the rotational transition in absence of any hyperfine interaction or external field, and the hyperfine coupling constants $(eqQ)_1$, $(eqQ)_2$, C_1, C_2 and d_T.

Because the total angular momentum quantum number F is a good quantum number, the energy matrix factorizes into submatrices corresponding to the allowed values of F. The quadrupole coupling constant of the halide nucleus has a very high value and the interaction between the quadrupole moment of this nucleus and the field gradient couples states with J values differing by two. In the case of the $J = 0 \rightarrow 1$ transition, we take into account the contribution of the $J = 2$ states for the level $J = 0$, and of the $J = 3$ states for the level $J = 1$.

In the order to calculate the energy splitting of a rotational level, the hyperfine matrices are diagonalized. The initial values for the rotational and hyperfine constants are either values from previous measurements or estimated values. From the diagonalized energy matrices and the calculated relative intensities, the hyperfine spectrum is obtained and compared with the measured spectrum. In the next stage the values of the constants are varied until the best set of values is obtained, which reproduced the experimental line frequencies fairly well. Finally, starting from this set of values a least square method (BLU 68) is applied to obtain the best-fit constants with their errors. The calculations are carried out on a IBM 360/50 digital computer of the University.

4.1.2 *HFS in the $J = 0 \rightarrow 1$ transition of HI, HBr and DBr*

The submillimeter wave power for the $J = 0 \rightarrow 1$ transition of $H^{127}I$ at 385 GHz is the 6th harmonic of 64.2 GHz. Table 4.1 summarizes the observed

[1] The gases HI and HBr were obtained from The Matheson Company, East Rutherford (U.S.A.), and DBr from The Nuclear Equipment Chemical Corporation, Farmingdale (U.S.A.).

frequencies of the hyperfine components of $H^{127}I$. The halfwidth is 6.5 kHz. In the earlier measurements on the same transition of HI by Cowan and Gordy (COW 56) the halfwidth was about 250 kHz. The frequency ν_0, the rotational constant and the hyperfine coupling constants of $H^{127}I$ are given in Table 4.2. The rotational constant has been calculated from the frequency ν_0 and the centrifugal distortion constant $D_0 = (6.21 \pm 0.12)$ MHz obtained from the infrared spectrum by Hurlock *et al* (HUR 71). Comparison between observed frequencies and frequencies calculated with the best-fit constants of Table 4.2 shows a maximum deviation of 0.2 kHz. This demonstrates the quality of the fit which is achieved.

The submillimeter wave power for the $J = 0 \rightarrow 1$ transition of $H^{79}Br$ and $H^{81}Br$ at 500 GHz is the 5th harmonic of 100 GHz. A recording of the doublet of $H^{81}Br$ $(F_1; F) = (3/2; 1,2) \rightarrow (F_1'; F') = (1/2; 0), (1/2; 1)$ is given in Fig. 4.1.

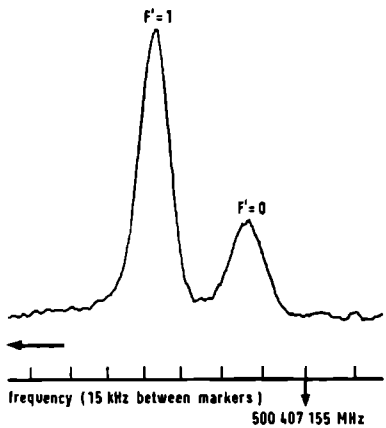

FIG. 4.1 Recording of the $F_1 = 3/2 \rightarrow 1/2$ hyperfine components of the $J = 0 \rightarrow 1$ rotational transition of $H^{81}Br$.

A better accuracy than that shown in this figure is obtained by using an extended frequency scale (5 kHz between markers). The halfwidth is 7.5 kHz. Table 4.3 summarizes the observed frequencies of the hyperfine components of $H^{79}Br$ and $H^{81}Br$. The frequency ν_0, the rotational constant and the hyperfine coupling constants of $H^{79}Br$ and $H^{81}Br$ are given in Table 4.4. The rotational constant B_0 has been calculated from the frequency ν_0 and the centrifugal distortion constant $D_0 = (10\,315.9 \pm 3.0)$ kHz and $D_0 = (10\,309.6 \pm 3.0)$ kHz for $H^{79}Br$ and $H^{81}Br$, respectively, obtained from the infrared spectrum by Rank *et al* (RAN 65). Comparison between observed frequencies and frequencies calcula-

ted with the best-fit constants of Table 4.4 shows a maximum deviation of 0.15 kHz.

The millimeter wave power for the $J = 0 \rightarrow 1$ transition of $D^{79}Br$ and $D^{81}Br$ at 254.5 GHz is the 4th harmonic of 63.6 GHz. Table 4.5 summarizes the observed frequencies of the hyperfine components of $D^{79}Br$ and $D^{81}Br$. The two lines of the $F_1 = 1/2 \rightarrow 1/2$ component of the transition overlap and are measured as one line. Since it is known, that these lines have relative intensities 1 : 2, and that their separation from the measured frequency is $(2/3)\ (C_D - d_T)$ and $(-1/3)\ (C_D - d_T)$, respectively, we are able to determine them. The halfwidth of the lines is 5.5 kHz. The frequency ν_0, the rotational constant and the hyperfine coupling constants of $D^{79}Br$ and $D^{81}Br$ are given in Table 4.6. The rotational constant has been calculated from the frequency ν_0 and the centrifugal distortion constant $D_0 = (2.89 \pm 0.05)$ MHz and $D_0 = (2.88 \pm 0.05)$ MHz for $D^{79}Br$ and $D^{81}Br$, respectively, obtained from the infrared spectrum by Keller and Nielsen (KEL 53). Comparison between observed frequencies and frequencies calculated with the best-fit constants of Table 4.6 shows a maximum deviation of 0.50 kHz.

TABLE 4.1 Observed frequencies of the $J = 0 \rightarrow 1$ rotational transition of $H^{127}I$.

Transition $F_1 ; F \rightarrow F_1' ; F'$		Relative Intensity	Frequency (MHz)
	3/2 2	5	385 545.1795 (3)
	3/2 1	3	385 545.1342 (3)
5/2; 2, 3	7/2 3	7	385 382.7104 (2)
	7/2 4	9	385 382.6602 (2)
	5/2 2	5	384 997.5456 (2)
	5/2 3	7	384 997.5146 (2)

TABLE 4.2 Rotational constant, hyperfine coupling constants, and frequency ν_0 of the transition $J = 0 \rightarrow 1$ of HI. All values are in kHz.

	Present measurement	Other measurement	Reference
ν_0	385 290 339.2 (2)	385 293 270 (700)	(COW 56)
B_0	192 657 590 (480)	192 658 800 (500)	(COW 56)
$(eqQ)_I$	−1 828 286.1 (8)	−1 831 000 (1000)	(COW 56)
C_I	351.03 (5)	260 (200)	(COW 56)
C_H	−49.36 (22)	−49.7 (10)	(RAM 61)
d_T	5.51 (10)		

TABLE 4.3 Observed frequencies of the J = 0 → 1 rotational transition of HBr.

	Transition F_1 ; $F \rightarrow F_1'$; F'	Relative intensity	Frequency (MHz)
$H^{79}Br$	3/2; 1, 2 1/2 0	1	500 540.1020 (5)
	1/2 1	3	500 540.1362 (3)
	5/2 3	7	500 647.7273 (3)
	5/2 2	5	500 647.7696 (3)
	3/2 2	5	500 780.0831 (3)
	3/2 1	3	500 780.1233 (3)
$H^{81}Br$	3/2; 1, 2 1/2 0	1	500 407.1747 (5)
	1/2 1	3	500 407.2096 (3)
	5/2 3	7	500 497.3676 (3)
	5/2 2	5	500 497.4092 (3)
	3/2 2	5	500 607.7590 (3)
	3/2 1	3	500 607.8007 (3)

TABLE 4.4 Rotational constant, hyperfine coupling constants, and frequency ν_0 of the rotational transition J = 0 → 1 of HBr. All values are in kHz.

	Present measurement	Other measurement	Reference
$H^{79}Br$			
ν_0	500 673 918.8 (2)	500 675 240 (260)	(JON 64b)
B_0	250 357 519 (12)	250 360 780 (130)	(JON 64b)
$(eqQ)_{Br}$	532 304.1 (8)	535 400 (1400)	(JON 64b)
C_{Br}	290.83 (8)	290 (200)	(JON 64b)
C_H	−41.27 (31)	−43 (3)	(RAM 61)
d_T	10.03 (21)		
$H^{81}Br$			
ν_0	500 519 145.5 (2)	500 519 410 (260)	(JON 64b)
B_0	250 280 192 (12)	250 282 880 (130)	(JON 64b)
$(eqQ)_{Br}$	444 679.3 (8)	447 900 (1400)	(JON 64b)
C_{Br}	313.25 (8)	310 (200)	(JON 64b)
C_H	−41.23 (31)	−43 (3)	(RAM 61)
d_T	10.89 (21)		

TABLE 4.5 Observed frequencies of the J = 0 → 1 rotational transition of DBr.

	Transition F_1 ; F ⟶ F_1' ; F′	Relative intensity	Frequency (MHz)
$D^{79}Br$	3/2; 1/2, 3/2, 5/2 1/2 1/2	1	254 571.6545 (15)[a]
	1/2 3/2	2	254 571.6593 (15)[a]
	5/2 3/2	2	254 678.3362 (15)
	5/2 7/2	4	254 678.3442 (10)
	5/2 5/2	3	254 678.3785 (5)
	3/2 3/2	2	254 810.6345 (5)
	3/2 5/2	3	254 810.6580 (5)
	3/2 1/2	1	254 810.6907 (5)
$D^{81}Br$	3/2; 1/2, 3/2, 5/2 1/2 1/2	1	254 437.7305 (15)[b]
	1/2 3/2	2	254 437.7358 (15)[b]
	5/2 3/2	2	254 526.9935 (15)
	5/2 7/2	4	254 527.0002 (10)
	5/2 5/2	3	254 527.0342 (5)
	3/2 3/2	2	254 637.4216 (5)
	3/2 5/2	3	254 637.4446 (5)
	3/2 1/2	1	254 637.4781 (5)

[a] These two lines overlap and are measured as one line with frequency 254 571.6577 (5) MHz.
[b] Same as[a]. Measured frequency 254 437.7340 (5) MHz.

TABLE 4.6 Rotational constant, hyperfine coupling constants, and frequency ν_0 of the rotational transition J = 0 → 1 of DBr. All values are in kHz.

	Present measurement	Other measurement (GOR 54)
$D^{79}Br$		
ν_0	254 704 657.1 (4)	254 705 200 (500)
B_0	127 358 110 (200)	127 358 200 (300)
$(eqQ)_{Br}$	530 631.5 (21)	533 000 (3000)
C_{Br}	145.82 (24)	
$(eqQ)_D$	146.9 (19)	
C_D	−3.25 (57)	
d_T	1.59 (24)	
$D^{81}Br$		
ν_0	254 548 931.2 (4)	254 548 900 (500)
B_0	127 280 220 (200)	127 280 000 (300)
$(eqQ)_{Br}$	443 279.9 (21)	445 000 (3000)
C_{Br}	157.26 (24)	
$(eqQ)_D$	146.1 (19)	
C_D	−3.55 (57)	
d_T	1.74 (24)	

4.2.1 *Calibration of the Stark field*

For the measurement of the Stark splittings a well-defined dc voltage (from Fluke 410 B, stability 1×10^{-4}) was applied to one plate and a negative square-wave voltage to the other plate. The latter voltage (frequency 1 kHz) modulates the absorption signals as required for the synchronous detection. The Stark components are measured during the zero-period of the square-wave.

During the initial stage of the Stark measurements on DBr at high fields it was found that the spectral lines were asymmetric. This asymmetry was ascribed to a slight variation of the distance between the (metal) Stark plates, especially between the middle and the end sections of the plates. A solution was found in using only the middle section, about 10 cm long, of the effuser during the Stark measurements. In this way, only the middle section of the parallel plates cell, where the plates are parallel to within less than 0.01 mm, is used for the absorption experiments. No asymmetry of the lines could be detected with this arrangement.

The well-known (MUE 68; LEE 70) dipole moment of carbonyl sulphide $\mu(OCS) = 0.71512(5)$ D was used to calibrate the Stark field.

The calibration was performed by measuring Stark splittings of the $J = 7 \rightarrow 8$ rotational transition at 97.3 GHz. All nuclear spins of the nuclei of normal OCS are zero, so the OCS molecule has no hyperfine structure. The first order Stark effect is zero. With the aid of the expression for the matrix elements of the $-\mu.\mathbf{E}$ interaction given in Eq. (3.15), the second order perturbation theory gives the following energy splitting of the rotational level J:

$$W_{JM}^{(2)}(\mu) = \frac{\mu^2 E^2}{2hB_0}\left[\frac{J(J+1) - 3M^2}{J(J+1)(2J-1)(2J+3)}\right] \tag{4.1}$$

The polarizability term $-\frac{1}{2}\mathbf{E}.\alpha.\mathbf{E}$ of Eq. (3.16) gives the following contribution to the first order energy:

$$W_{JM}^{(1)}(\alpha) = -\tfrac{1}{2}\alpha_S E^2 - \alpha_T E^2\left[\frac{3M^2 - J(J+1)}{(2J+3)(2J-1)}\right] \tag{4.2}$$

The scalar contribution of the polarizability drops out the transition frequencies. For OCS, the polarizability anisotropy is $(\alpha_{//} - \alpha_\perp) = 4.63 \times 10^{-24}$ cm^3 (MUE 68), and the rotational constant $B_0 = 6081.490$ MHz (TOW 55).

Both contributions (4.1) and (4.2) are quadratic in the electric field. There

are three perturbation corrections which have a fourth power dependence on the applied electric field, and expressions for them are given in the appendix of the paper of Scharpen *et al* (SCH 67). For the applied electric fields in this experiment, these corrections are negligible (DIJ 69).

The microwave electric field is parallel to the static electric field, so the rotational transitions produced by the electric field can occur only when $\Delta M = 0$. In Table 4.7 the observed frequencies of the Stark components of the rotational transition $J = 7 \rightarrow 8$ of OCS are given for a number of dc voltages in the range 3000–4000 V and for the square-wave voltage of —500 V. The halfwidth of the lines is about 3.8 kHz.

TABLE 4.7 Frequencies of the rotational transition $J = 7 \rightarrow 8$ of OCS in a Stark field. The error in the frequencies is 0.30 kHz.

quantum number M	observed frequencies (kHz) at different dc voltages		
	2996.3 V	3495.7 V	3995.4 V
2	97 301 146.01	97 301 123.28	97 301 097.24
4	97 301 258.94	97 301 277.13	97 301 298.38
5	97 301 343.89	97 301 392.82	97 301 448.81
6	97 301 447.94	97 301 534.02	97 301 633.37
7	97 301 570.47	97 301 700.93	97 301 851.66

From the observed frequencies at the three values of the dc voltage the values of the electric field and of the frequency ν_0 of the rotational transition $J = 7 \rightarrow 8$ of OCS at zero Stark field are obtained by means of a least squares fit method. The values of the frequency ν_0 show a maximum deviation of 0.05 kHz from the averaged value of $\nu_0 =$ 97 301 208.49 (12) kHz. From the values for the electric field and the applied dc voltage we obtain the distance d of the parallel plates: $d = (0.98411 \pm 0.00023)$ cm. The d-values determined at different applied voltages are consistent within the indicated error limit. This demonstrates together with the result obtained for the frequency the reliability of the calibration method. Consequently, we know the electric field for each value of the dc voltage applied on the parallel plates.

4.2.2 *Stark effect in the $J = 0 \rightarrow 1$ transition*

a HBr and DBr

At the same conditions as used for the calibration of the Stark field with OCS, the Stark splitting of the rotational transition $J = 0 \rightarrow 1$ of the molecules $H^{79}Br$,

$H^{81}Br$, $D^{79}Br$ and $D^{81}Br$ is measured For these molecules all Stark measurements were performed only on the transition $(J, F_1) = (0,3/2) \rightarrow (1, 1/2)$ The diagonal contribution of α_T is exactly zero for the $J = 0$ level and for the $(1, 1/2)$ hyperfine sublevels

The splitting pattern of the $(J, F_1) = (0, 3/2) \rightarrow (1, 1/2)$ transition of HBr consists of two lines for both isotopic species These lines correspond to the transition $(J, F_1, M_1, M_2) = (0, 3/2, -1/2, 1/2) \rightarrow (1, 1/2, -1/2, 1/2)$ and to the degenerate pair of transitions $(0, 3/2, 1/2, 1/2) \rightarrow (1, 1/2, 1/2, 1/2)$ and $(0, 3/2, 1/2, -1/2) \rightarrow (1, 1/2, 1/2, -1/2)$. The separation between them is independent of the applied Stark field and is 34 2 kHz for $H^{79}Br$ and 34 8 kHz for $H^{81}Br$. The results are given in Table 4 8

TABLE 4 8 Observed frequencies of the stronger Stark component of the $(J, F_1) = (0,3/2) \rightarrow (1,1/2)$ transition of HBr and the corresponding values of the electric dipole moment

	Stark field (V/cm)	observed frequency (MHz)	dipole moment (D)
$H^{79}Br$	0	500 540 1362 (3)	
	3044 7 (8)	500 541 2048 (10)	0 82709 (47)
	3552 1 (9)	500 541 5897 (10)	0 82708 (37)
	4059 9 (11)	500 542 0335 (10)	0 82704 (32)
$H^{81}Br$	0	500 407 2096 (3)	
	3044 7 (8)	500 408 2799 (10)	0 82778 (47)
	3552 1 (9)	500 408 6638 (10)	0 82736 (37)
	4059 9 (11)	500 409 1070 (10)	0 82720 (32)

The $(J, F_1) = (0, 3/2) \rightarrow (1, 1/2)$ transition of DBr without Stark field is observed as a single line, containing in fact two overlapping lines (Table 4.5). At Stark field the line shifts keeping the same structure The results are given in Table 4 9.

TABLE 4 9 Observed frequencies of the $(J, F_1) = (0,3/2) \rightarrow (1,1/2)$ Stark transition of DBr and the corresponding values of the electric dipole moment

	Stark field (V/cm)	observed frequency (MHz)	dipole moment (D)
$D^{79}Br$	0	254 571.6577 (5)	
	3044 7 (8)	254 573 7377 (10)	0 82353 (31)
	3552 1 (9)	254 574 4852 (14)	0 82351 (31)
	4059 9 (11)	254 575 3452 (18)	0 82338 (30)
$D^{81}Br$	0	254 437 7340 (5)	
	3044 7 (8)	254 439 8133 (10)	0 82346 (31)
	3552 1 (9)	254 440 5598 (14)	0 82342 (31)
	4059 9 (11)	254 441 4168 (18)	0 82312 (30)

With μ as parameter and all other constants taken from the measurements at zero Stark field the energy matrices are diagonalized and the transition frequencies of the Stark spectrum are calculated. Comparison between calculated and observed frequencies gives values for μ at the three E values (Table 4.8; Table 4.9). The final results for the electric dipole moments are:

$$\mu\,(H^{79}Br) = 0.8271\ (3)\ D$$
$$\mu\,(H^{81}Br) = 0.8274\ (3)\ D$$
$$\mu\,(D^{79}Br) = 0.8235\ (3)\ D$$
$$\mu\,(D^{81}Br) = 0.8233\ (3)\ D$$

In these measurements the isotope effect of the $H \rightarrow D$ substitution for the dipole moment of hydrogen-bromide has been observed for the first time, but the present accuracy is too low to determine the effect of the $^{79}Br \rightarrow {}^{81}Br$ substitution. The value for HBr is higher than the value 0.788 D obtained by Zahn (ZAH 24) from measurements on the dielectric constant, but it agrees well with the value 0.834 ± 0.008 D obtained by Robinette and Sanderson (ROB 69) from measurements on far infrared dispersion. The value for DBr agrees well with the value 0.83 ± 0.02 D obtained by Burrus (BUR 59) from a low-resolution Stark effect measurement on the $J = 0 \rightarrow 1$ transition of this molecule.

b HI

For $H^{127}I$ all Stark measurements were performed on the transition $(J, F_1) = (0, 5/2) \rightarrow (1, 7/2)$. These measurements have been done under slightly differing conditions: the length of the effuser was 39 cm, Stark fields between 2000–3000 V, and the square wave voltage of —2000 V. The calibration of the Stark field with OCS has been performed also under these conditions.

In the case of the (1, 7/2) level of HI the largest contributions of α_T are for the $M_1 = 1/2, 7/2$; they are $+(1/7)\alpha_T E^2/h$ and $-(1/5)\alpha_T E^2/h$, respectively. The only known source of information on α_T of HI are the tables of Landolt-Börnstein (LAN 51) which give:

$\alpha_T(HI) = -0.563 \times 10^{-24}$ cm^3. With this value of α_T the shift of the $M_1 = 1/2, 7/2$ sublevels is —1.2 and 1.7 kHz, respectively, at an electric field of 3000 V/cm. However, recent measurements of Bridge and Buckingham (BRI 66) on HCl suggest that the α_T values for halide-hydrides of Landolt-Börnstein are overestimated by roughly a factor of two. If this is correct even the largest contributions of α_T are well below the present limit ($\simeq$ 1 kHz) of the fit accuracy. Consequently we felt that it was not justified to attempt extraction of α_T from

our measurements and the contribution of α_T was disregarded in the analysis.

The observed and the calculated Stark splitting pattern of the $(J, F_1) = (0, 5/2) \rightarrow (1, 7/2)$ of HI at E = 2044.4 V/cm is shown in Fig. 4.2. At this field the maximum shift of a component from the unsplit line is about 220 kHz.

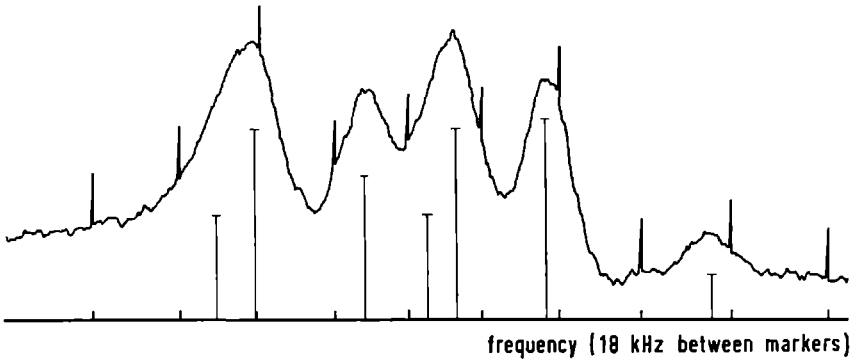

FIG. 4.2 The observed (recording) and the calculated (bars) Stark splitting pattern of the $(J, F_1) = (0,5/2) \rightarrow (1, 7/2)$ transition of HI at F = 2044.4 V/cm

The halfwidth of a single component is 7.0 kHz. The calculated pattern was obtained from the best fit of the observed spectra to the Hamiltonian of Eq. (3.4) with μ as the only fit parameter. The other constants required for the fit were taken from the measurements at zero Stark field.

The value of the electric dipole moment is obtained from the fit of a number of observed spectra at six values of E in the range of 2–3 kV/cm. The result is:

$$\mu(H^{127}I) = 0.4477(5) \text{ D}$$

A detailed description of the Stark measurement on HI and its computer fit is given by Zuidberg (ZUI 69).

Thus far the only value for the dipole moment of HI is the value 0.382 D obtained by Zahn (ZAH 24) from measurements of the dielectric constant. The value obtained in the present measurement is higher than Zahn's value, just like that of HBr. The value agrees well with the value of $\mu(DI) = 0.445 \pm 0.02$ D obtained by Burrus (BUR 59) from a low-resolution Stark effect measurement on the $J = 0 \rightarrow 1$ transition of DI.

DISCUSSION OF THE RESULTS

5 1 VIBRATIONAL DEPENDENCE OF MOLECULAR CONSTANTS

For a $^1\Sigma$-diatomic molecule in the vibration-rotation state vJ the expectation value of an arbitrary operator **O** which is a known function of the internuclear distance R, can be expanded as a Taylor series for values of R in the neighbourhood of R_e:

$$< \mathbf{O} >_{vJ} = O_e - O_1 < \zeta > + \tfrac{1}{2} O_2 < \zeta^2 > + \tfrac{1}{6} O_3 < \zeta^3 > + \ldots \qquad (5\,1)$$

where $O_n = R_e{}^n (d^n O/dR^n)_e$,
$\zeta = (R - R_e)/R_e$

For the Dunham potential function given in Eq (3 1) the expectation value of ζ^n is a function of J, $v + \frac{1}{2}$, (B_e/ω_e), and of the potential constants a_i (SCH 61) The constants R_e, B_e, ω_e, and a_i are known for nearly all simple molecules from rotation and vibration spectra They are given in Table 5 1 for the hydrogen-halides Omitting terms of third and higher order in (B_e/ω_e) the following equation is obtained for the expectation value of **O**.

$$\begin{aligned} < \mathbf{O} >_{vJ} &= O_e + (B_e/\omega_e)\,(v + \tfrac{1}{2})\,[-3a_1 O_1 + O_2] - \\ &+ (B_e/\omega_e)^2\,[O_1\,(-\tfrac{15}{4} a_3 + \tfrac{23}{4} a_1 a_2 - \tfrac{21}{8} a_1{}^3 + \\ &+ O_2(-\tfrac{3}{4} a_2 + \tfrac{7}{8} a_1{}^2) - \tfrac{7}{24} a_1 O_3 + \tfrac{1}{16} O_4] + (B_e/\omega_e)^2\,(v + \tfrac{1}{2})^2 \times \\ &\times [O_1(-15\, a_3 + 39\, a_1 a_2 - \tfrac{45}{2} a_1{}^3) + O_2(-3a_2 + \tfrac{15}{2} a_1{}^2) - \tfrac{5}{2} a_1 O_3 + \tfrac{1}{4} O_4] + \\ &+ (B_e/\omega_e)^2\, 4J(J + 1) O_1 \end{aligned} \qquad (5\,2)$$

From above expression it is apparent that by measuring only the vibrational variation of the expectation value of an operator, one is not able to determine the individual derivatives of the operator The first derivative can be obtained from the last term of Eq (5 2), if the centrifugal distortion within a vibrational level is observable, while the second derivative can also be determined, if the coefficient of the term $(B_e/\omega_e)\,(v + \frac{1}{2})$ is known from the vibrational variation of the expectation value

TABLE 5.1 Molecular constants of hydrogen-halides.

Quantity	HF	$H^{35}Cl$	$H^{81}Br$	HI
R_e(°A)	0.91681[a]	1.2746[b]	1.4146[b]	1.6091[b]
B_e(cm^{-1})	20.9557[a]	10.593416[c]	8.464884[d]	6.5111[e]
ω_e(cm^{-1})	4138.32[a]	2990.9463[c]	2648.975[d]	2309.014[e]
a_1	−2.2537[a]	−2.3645[c]	−2.4373[d]	−2.533[f]
a_2	3.4880[a]	3.66470[c]	3.8645[d]	
a_3	−4.4987[a]	−4.6783[c]	−5.151[d]	

[a] Reference WEB 68, [b] Reference JON 64b, [c] Reference RAN 65a, [d] Reference RAN 65, [e] Reference HUR 71, and [f] $a_1 = (-\alpha_e\omega_e/6B_e^2)$—1 (TOW 55, p. 16) with $\alpha_e = 0.16886$ cm^{-1} (HUR 71).

With the values of the molecular constants given in Table 5.1 the coefficients in Eq. (5.2) can be calculated. It turns out that the terms in $(B_e/\omega_e)^2$ are about 100× smaller than the term in (B_e/ω_e) for low values of v and J. Consequently, it is sufficient in first approximation to retain only terms through order (B_e/ω_e) in Eq. (5.2). Then the vibrational dependence of the expectation value of an operator can be obtained by measuring it in the ground and in the first excited vibrational state.

In the present investigation the measurements have been done only for the ground vibrational state of the molecules, because the fraction of the molecules in an excited vibrational state at room temperature is too small for the beam spectrometer. However, separation of the equilibrium value O_e and of the vibration-dependent part, $\frac{1}{2}(B_e/\omega_e)\,[-3a_1O_1 + O_2]$, of the expectation value of **O** can also be achieved by the method of isotopic substitution.

5.2 EFFECT OF ISOTOPIC SUBSTITUTION

If a nucleus A in a hydrogen-halide molecule is replaced by its isotope B, the molecular quantities R_e, O_e, O_1, O_2, and a_i's are influenced by the change in the electronic wave function resulting from the different volumes of the two isotopic nuclei. This change is very small and it is neglected in the following. Furthermore isotopic substitution changes the vibration of the molecule in consequence of the different masses of the two isotopic nuclei. Assuming that the Born-Oppenheimer approximation is valid, the electronic wave function and, subsequently, the molecular quantities mentioned above are not influenced by this change in vibration. With these assumptions we obtain from Eq. (5.2) by neglecting second and higher order terms in (B_e/ω_e) the following expression

for the difference in the expectation values of an operator **O** on isotopic substitution:

$$< \mathbf{O} >_{v,B} - < \mathbf{O} >_{v,A} = (v + \tfrac{1}{2})\,(B_e/\omega_e)_A\,[-3a_1O_1 + O_2] \times$$
$$\times\,[(\mu_{M,A}/\mu_{M,B})^{\frac{1}{2}} - 1] \qquad (5.3)$$

Herein μ_M is the reduced mass of a molecule, and A and B denote two molecules differing only by one isotopic substitution. In order to obtain Eq. (5.3) we have used the property that the quantity (B_e/ω_e) is proportional to $\mu_M^{-\frac{1}{2}}$.

Because we have measured the molecular constants in the ground ($v = 0$) vibrational state only, we use in the following the notation $< \mathbf{O} >_0 = O$. In fact this notation has been used already in chapters 3 and 4.

5.3 QUADRUPOLE COUPLING CONSTANTS

5.3.1 *The vibrational dependence of the quadrupole coupling constant of the Cl-nucleus in HCl and DCl*

Kaiser (KAI 70) has observed the values of the quadrupole coupling constant $(eqQ)_{Cl}$ in the molecule $H^{35}Cl$ and $D^{35}Cl$ as function of $(v + \frac{1}{2})$ and J. Consequently, we can compare for $H^{35}Cl$ the results obtained with the isotopic substitution method with results obtained more directly by measuring vibrational and rotational dependence.

Using Eq. (5.2) Kaiser obtained the following results for $H^{35}Cl$: $(eqQ)_e = -66775.1 \pm 3.0$ kHz, and $(B_e/\omega_e)\,[-3a_1\,(eqQ)_1 + (eqQ)_2] = -1672.8 \pm 6.4$ kHz. With the aid of the method of isotopic substitution applied to the values of $(eqQ)_{Cl}$ ($v = 0$) in $H^{35}Cl$ and $D^{35}Cl$, we obtain the following result for $H^{35}Cl$: $(eqQ)_e = -66821$ kHz and $(B_e/\omega_e)\,[-3a_1\,(eqQ)_1 + (eqQ)_2] = -1595$ kHz. In the latter calculation all terms in $(B_e/\omega_e)^2$ were neglected. The agreement between the results obtained with the two different methods is reasonable. So it may be concluded that the method of isotopic substitution to determine the vibrational dependence of the quadrupole coupling constant of HCl is very well. Therefore this method will be used in order to determine the vibrational dependence of the quadrupole coupling constant and of other quantities of HBr.

With the aid of Eq. (5.2) and a value for the quadrupole moment of the ^{35}Cl-nucleus Kaiser determined also values for q_e, q_1 and q_2 for the Cl-nucleus in $H^{35}Cl$ and $D^{35}Cl$. The results for $H^{35}Cl$ are given in Table 5.2 (Sect. 5.3.2). The results for $D^{35}Cl$ are identical to the results for $H^{35}Cl$ within the experimental error. This legitimates one of the assumptions mentioned in Sect. 5.2.

5.3.2 *Field gradient at the Br-nucleus in HBr and DBr*

Starting from the value of the nuclear electric quadrupole moment $Q(^{81}Br) = 0.26 \times 10^{-24}$ cm^2 (FUL 65), we obtain from the observed quadrupole coupling constant $(eqQ)_{Br}$ the field gradient $q = 7.073321\ (13) \times 10^{22}$ V/m^2 and $q = 7.051061\ (34) \times 10^{22}$V/m^2 for the Br-nucleus in $H^{81}Br$ and $D^{81}Br$, respectively, in the ground vibrational state.

Using the method of isotopic substitution we obtain from Eq. (5.3) and from the values of the field gradient in $H^{81}Br$ and $D^{81}Br$ the value of the vibration-dependent part of the field gradient for the Br-nucleus in $H^{81}Br$:

$$\tfrac{1}{2}(B_e/\omega_e)\,[-3a_1q_1 - q_2] = (7.72 \pm 0.02) \times 10^{20}\ \text{V/m}^2 \qquad (5.4)$$

By substituting the value of q and of $\frac{1}{2}(B_e/\omega_e)\,[-3a_1q_1 + q_2]$ into Eq. (5.2) and neglecting the terms of the order $(B_e/\omega_e)^2$, we obtain the value of q_e for the Br-nucleus in $H^{81}Br$. The results are given in Table 5.2 both for Br in $H^{81}Br$ and $D^{81}Br$, and in $H^{79}Br$ and $D^{79}Br$.

We can solve Eq. (5.4) for q_1 if we assume that the value of q_1/q_2 for the Br-nucleus in $H^{81}Br$ is the same as for the Cl-nucleus in $H^{35}Cl$ (Table 5.2). The values of the constants B_e, ω_e and a_1 for $H^{81}Br$ are given in Table 5.1. The result for q_1 and, subsequently, for q_2 is given in Table 5.2. In order to determine the error in q_1 we compare the value of q_e/q_1 for the Br-nucleus in $H^{81}Br$ with this ratio for the Cl-nucleus in $H^{35}Cl$. The difference in these ratios is only 6 %. Therefore, estimating the accuracy of q_1 and q_2 as 10 % and 20 %, respectively, seems reasonable taking into account the uncertainties involved in the isotopic substitution method. The accuracy of q_e has been determined on 7×10^{-4} as suggested in the treatment of HCl in Sect. 5.3.1.

TABLE 5.2 Field gradient and its derivatives of the halide nucleus in HBr and HCl.

	HBr (present work)	$H^{35}Cl$ (KAI 70)
q_e(V/m^2)	6.996(5) × 10^{22}	3.5313(3) × 10^{22}
q_1(V/m^2)	9.6(10) × 10^{22}	5.17(21) × 10^{22}
q_2(V/m^2)	−22(5) × 10^{22}	−11.6(16) × 10^{22}

5.3.3. *Field gradient at the D-nucleus in DBr*

The vibrational dependence of $(eqQ)_D$ in $D^{81}Br$ and $D^{79}Br$ can not be determined, because the difference in the vibrational dependence of $(eqQ)_D$ in the

two isotopic species of this molecule is considerably smaller than the present accuracy. Therefore the values for $(eqQ)_D$ of $D^{81}Br$ and $D^{79}Br$ may be averaged with as result: $(eqQ)_D = 146.5$ (14) kHz for DBr. Starting from the value of the nuclear electric quadrupole moment $Q(D) = 0.00277 \times 10^{-24}$ cm^2 we obtain from $(eqQ)_D$ the field gradient $q = 2.16 \times 10^{21}$ V/m^2 for the D-nucleus in the ground vibrational state.

5.3.4 *Nuclear quadrupole ratio of Br isotopes in molecular HBr and DBr*

From the observed quadrupole coupling constant $(eqQ)_{Br}$ in $H^{81}Br$ and $H^{79}Br$ (Table 4.4), we can determine the ratio $(eq_{79}Q_{79})/(eq_{81}Q_{81}) = 1.197052$ (3). The difference in the ratio of the quadrupole coupling constants for $v = 0$ and in the ratio of the quadrupole coupling constants for the equilibrium distance R_e is smaller than 2×10^{-6}. In order to prove this we used $(B_e/\omega_e)_{79}/(B_e/\omega_e)_{81} = 1.00015$ (RAN 65).

So we obtain for $(eq_{79}Q_{79})_e/(eq_{81}Q_{81})_e = 1.197052$ (5). Assuming $(q_{79})_e = (q_{81})_e$ we obtain for the nuclear quadrupole ratio of the bromine isotopes in HBr: $Q_{79}/Q_{81} = 1.197052$ (5). For DBr the ratio is 1.197057 (10). These results are in very good agreement with the value obtained by Hebert and Street (HEB 69) from the spectrum of LiBr, and by Brown and King (BRO 66) from the spectrum of atomic Br. Consequently, no indication is found of the nuclear polarizability effect.

After publications of these experimental results (BRO 66, HEB 69, DIJ 69) Bonczyk (BON 70) has also given an explanation for the failure to observe an electric polarization effect of $^{79,81}Br$ nuclei.

5.4 ELECTRIC DIPOLE MOMENTS

5.4.1 *The vibrational dependence of the dipole moment of HCl and DCl*

Kaiser (KAI 70) has found that the value for the dipole moment μ_e of $H^{35}Cl$ for the equilibrium distance R_e is (0.001 ± 0.0002) D greater than the value for $D^{35}Cl$. This difference in μ_e for HCl and DCl is ascribed to breakdown of the Born-Oppenheimer approximation. Kaiser has obtained the value of μ_e, μ_1, μ_2, μ_3, and μ_4 for HCl and DCl from a calculation in which he used the 'wavefunction approximation', dipole matrix elements obtained from measurements of absolute intensities of the infrared spectra of HCl and DCl, and his own measurements on the dipole moment of HCl and DCl in different vibrational states. Two results for $H^{35}Cl$ are relevant in this section: $\mu_e = 1.0933$ D, and the vibration-dependent part $\frac{1}{2}(B_e/\omega_e)\,[-3a_1\mu_1 + \mu_2] = 0.0152$ D.

These quantities can also be determined with the method of isotopic substitution. In order to take into account the breakdown of the Born-Oppenheimer approximation, the difference in the equilibrium dipole moments of the two molecules differing by one isotopic substitution must be added to the right hand side of Eq. (5.3). Then we obtain the following equation for the difference of the dipole moments of two isotopic species of a molecule in the ground vibrational state:

$$\begin{aligned} &< \mu >_B - < \mu >_A = \\ &= \mu_{e,B} - \mu_{e,A} + \tfrac{1}{2}(B_e/\omega_e)_A \, [-3a_1\mu_1 + \mu_2] \, [(\mu_{M,A}/\mu_{M,B})^{\frac{1}{2}} - 1] \end{aligned} \tag{5.5}$$

From Eq. (5.5) and the observed dipole moments of HCl and DCl (KAI 70) we determine the following results for $H^{35}Cl$: $\mu_e = 1.0931$ D, and $\frac{1}{2}(B_e/\omega_e)$ $[-3a_1\mu_1 + \mu_2] = 0.0154$ D. The values obtained with the isotopic substitution method are in very good agreement with the values obtained with the method followed by Kaiser. So the isotopic effect can be used to determine the vibrational dependence of the dipole moment of HBr.

5.4.2 *Dipole moment functions of HBr and DBr*

The effect of the $^{79}Br \rightarrow {}^{81}Br$ substitution in HBr and DBr for the dipole moments can not be determined from the present experimental values. Therefore the values of the dipole moments of HBr and DBr for the bromine isotopes are averaged. The results are $\mu(HBr) = 0.82725$ (21) D, and $\mu(DBr) = 0.82340$ (21) D.

Assuming that the effect of the Born-Oppenheimer breakdown on μ is proportional to the value of the dipole moment, a difference in μ_e for HBr and DBr of 0.00075 D is deduced from Kaiser's results for HCl and DCl. Using the method of the isotopic substitution, we obtain from Eq. (5.5) for the vibration-dependent part of the dipole moment of HBr:

$$\tfrac{1}{2}(B_e/\omega_e) \, [-3a_1\mu + \mu_2] = (0.0108 \pm 0.0011) \text{ D} \tag{5.6}$$

Again omitting the terms of second and higher order in (B_e/ω_e) we obtain from Eq. (5.2) and the averaged value of $\mu(HBr)$ the value of μ_e for the HBr molecule. The result for μ_e is given in Table 5.2.

Babrov *et al* (BAB 65) have measured the electric dipole matrix elements for the 1 — 0 and 2 — 0 vibration-rotation bands of HBr and obtained subsequently the dipole moment derivatives μ_1 and μ_2. Rao and his collaborators (RAO 68; GUS 70) have remeasured the dipole matrix elements for these bands with a

higher resolution, so that the isotopic lines of $H^{79}Br$ and $H^{81}Br$ have been resolved. Tipping and Herman (TIP 70) obtained with a more sophisticated treatment the dipole moment function from the dipole matrix elements obtained by various experimentalists (BAB 65, RAO 68, GUS 70, BUR 59). The results are shown in Table 5.3. Tipping and Herman conclude that the data of Babrov *et al* are reasonably self-consistent, but those of Rao *et al* are not. They can not explain this discrepancy.

Therefore, it is interesting to compare the values of Tipping and Herman for the dipole moment derivatives with the values which can be derived from the present results using Eq. (5.6). The term μ_2 is small compared with the term $-3a_1\mu_1$ in Eq. (5.6). Taking $\mu_2 = 0.33$ D, a value suggested by Tipping and Herman, we obtain $\mu_1 = (0.88 \pm 0.10)$ D. This value does not agree with the values derived by Tipping and Herman (Table 5.3) either from the experimental results of Babrov *et al* (0.644 ± 0.006 D) or from Rao and collaborators (0.482 D).

TABLE 5.3 Electric dipole moment and its derivatives for HBr.

μ_e(D)		0.824 ± 0.02[d]	0.826[d]	0.8165 ± 0.0015[e]
μ_1(D)	0.645[a]	0.644 ± 0.006[b]	0.482[c]	0.88 ± 0.10[f]
$\frac{1}{2}\mu_2$(D)	0.069[a]	0.167 ± 0.06[b]	0.037[c]	

[a] Babrov *et al* (BAB 65); from line intensities of 1—0 and 2—0 vibration-rotation bands of HBr.
[b] Tipping and Herman (TIP 70); from data of Babrov *et al* (BAB 65).
[c] Tipping and Herman (TIP 70); from data of Rao and collaborators (RAO 68, GUS 70).
[d] Tipping and Herman (TIP 70); deduced from microwave spectroscopy (BUR 59) with different zero point corrections.
[e] Present work; $\mu_e = (0.81575 \pm 0.0015)$ D for DBr.
[f] Present work; with $\frac{1}{2}\mu_2$(D) = 0.167 D.

5.4.3 *Dipole moment function of HI*

In the present work only the dipole moment of $H^{127}I$ is measured. Benesch (BEN 64) obtained dipole matrix elements from infrared line intensities of HI and used them to determine the dipole derivatives (Table 5.4). If we substitute in Eq. (5.2) the values of μ (present work), and μ_1 and μ_2 of Benesch we obtain from this equation the value of μ_e. The second and higher order terms in (B_e/ω_e) in Eq. (5.2) were omitted again. The result is given in Table 5.4. We remark that for HI the value of μ_e is higher than the value of μ, in contrast with HBr (present work), HCl (KAI 70) and HF (MUE 70).

TABLE 5.4 Electric dipole moment and its derivatives for HI.

μ_e(D)	0.4483[a]
μ_1(D)	−0.082[b]
$\frac{1}{2}\mu_2$(D)	0.21[b]

[a] with μ_1 and $\frac{1}{2}\mu_2$ of Benesch (BEN 64).
[b] reference (BEN 64)

5.5 SPIN-ROTATION COUPLING CONSTANTS

5.5.1 *Vibrational dependence of the spin-rotation coupling constants of HBr and DBr*

a) Spin-rotation coupling constants of the Br-nucleus in HBr and DBr

The vibrational energy dependence of C_A, the spin-rotation coupling constant at nucleus A, can be written in the following form:

$$< C_A > = (C_A)_e + (v + \tfrac{1}{2})\,(B_e/\omega_e)\,[-3a_1\,(C_A)_1 + (C_A)_2] \qquad (5.7)$$

where we used Eq. (5.2) and neglected the terms of the order $(B_e/\omega_e)^2$. From the expressions given in Chap. 3 for the spin-rotation constant we may write:

$$(C_A)_e = g_A B_e a, \text{ and } -3a_1(C_A)_1 + (C_A)_2 = g_A B_e b$$

where B_e is the rotational constant at the distance R_e, g_A is the nuclear g factor of nucleus A, and a and b are molecular constants defined by these two equations. So Eq. (5.7) can be rewritten for the ground vibrational state as:

$$C_A = B_e g_A[a + \tfrac{1}{2}(B_e/\omega_e)b] \qquad (5.8)$$

At isotopic substitution $^{79}Br \rightarrow {}^{81}Br$ in HBr the quantity (B_e/ω_e) changes by about 1.5×10^{-4} but the molecular constants a and b do not change. The value of the term $\frac{1}{2}b(B_e/\omega_e)$ is about 3 % of the value of a (see below). So the total change of the term $a + \frac{1}{2}b(B_e/\omega_e)$ is about 5×10^{-6} at isotopic substitution of the Br-nucleus. This is a factor of 40 below the experimental accuracy of the C_{Br} constants in HBr. Consequently, from the observed value of the spin-rotation constant of the Br-nucleus in HBr, $C_{81} = 313.25$ (8) kHz, a new value of C_{79} can be calculated as follows:

$$C_{79} = (g_{79}B_{e79}/g_{81}B_{e81})C_{81} = 290.69\ (8)\ \text{kHz}$$

where the ratio $g_{79}/g_{81} = 0.9276997$ (3) is taken from a NMR measurement by Lutz (LUT 70), and $B_{e79}/B_{e81} = 1.0003114$ from the infrared spectrum

measured by Rank *et al* (RAN 65). The observed value of C_{79} is: C_{79} = 290 83 (8) kHz. The averaged of the two values is: C_{79} = 290.76 (6) kHz for the HBr molecule. The same procedure gives C_{79} = 145.81 (17) kHz for the DBr molecule.

Using the method of isotopic substitution for the H → D nucleus the vibration-dependent part of C_{79}, being the term $\frac{1}{2}b(g_{Br}B_e(B_e/\omega_e))_{79}$ equals 10.5 (12) kHz and 3 8 (5) kHz for HBr and DBr, respectively. The values of the spin-rotation constant at equilibrium internuclear distance $(C_{Br})_e$ are given in Table 5.5a.

b) Spin-rotation constants of the ^{1,2}H-nucleus in HBr and DBr

Within the measuring accuracy the C_H constants in $H^{79}Br$ and $H^{81}Br$ have the same value. The averaged value of $C_H(H^{79}Br)$ and $C_H(H^{81}Br)$ is C_H = —41.25 (22) kHz. For DBr the corresponding averaged value is C_D = —3.40 (40) kHz. The vibrational dependence of C_H for HBr can not be determined owing to the great error in the C_D value of DBr.

5.5.2 *Separation of nuclear and electronic contributions of the spin-rotation coupling constants in HBr and DBr*

The nuclear part of the spin-rotation coupling constant at the K-th nucleus at equilibrium internuclear distance is given by (Chap. 3):

$$C_{K,e}^{(n)} = -2e(\mu_0/4\pi)\mu_N g_K B_e R_e^{-1} \qquad (5.9)$$

The values obtained from this expression for $C_{Br,e}^{(n)}$ and $C_{H,e}^{(n)}$ of $H^{79}Br$ and $D^{79}Br$ are given in Table 5.5a, and 5 5b, respectively. The electronic part of the spin-rotation constant $C_{Br,e}^{(e)}$ at equilibrium internuclear distance can be obtained as the difference of $C_{Br,e}$—$C_{Br,e}^{(n)}$. This quantity is also given in Table 5.5a. Neglecting the vibrational dependence of the spin-rotation constant at the H-nucleus, we obtain the electronic part of the spin-rotation constant $C_H^{(e)}$ as the difference of $C_H - C_{H,e}^{(n)}$; this quantity is given in Table 5 5b. In accordance with the expectations the values in Table 5 5a and b yield: $(C_{Br,e}^{(e)}/B_e)_{HBr} = (C_{Br,e}^{(e)}/B_e)_{DBr}$, and $(C_H^{(e)}/g_H B_e)_{HBr} = (C_D^{(e)}/g_D B_e)_{DBr}$ within the present accuracy.

TABLE 5 5a Spin-rotation coupling constants of Br-nucleus in $H^{79}Br$ and $D^{79}Br$ (all values in kHz).

molecule	C_{Br}	$C_{Br,e}$	$C_{Br,e}^{(n)*}$	$C_{Br,e}^{(e)}$
$H^{79}Br$	290.76(6)	280 3(13)	—3.86	284.2(13)
$D^{79}Br$	145 81(17)	142 0(6)	—1.96	144.0(6)

TABLE 5.5b Spin-rotation coupling constants of the H-nucleus in $^1H^{79}Br$ and $^2H^{79}Br$ (= $D^{79}Br$) (all values in kHz).

molecule	C_H	$C_{H,\,e}{}^{(n)*}$	$C_H{}^{(e)}$
$^1H^{79}Br$	—41.25(22)	—15.4	—25.9
$^2H^{79}Br$	— 3.40(40)	— 1.20	— 2.20

* The nuclear g factors are given in the note of Table 5.6. The rotational constant $B_e(H^{79}Br)$ = 253.8 GHz (JON 64b) and $B_e(D^{79}Br)$ = 128.6 GHz (GOR 54).

5.6 SPIN-SPIN COUPLING CONSTANTS

The experimental value of the spin-spin coupling constant $d_T(exp)$ contains actually two terms:

$$d_T(exp) = d_T(nuclear) + d_T(electron\ coupled) \tag{5.10}$$

The term $d_T(nuclear)$ represents the nuclear spin-spin interaction and equals to (Chap. 3):

$$d_T(nuclear) = (\mu_0/4\pi)\mu_N{}^2 g_1 g_2 < R^{-3} >_v \tag{5.11}$$

In order to obtain the expectation value, R^{-3} is expanded in a Taylor series

$$< R^{-3} >_v = R_e{}^{-3}(1 - 3 < \zeta > + 6 < \zeta^2 > - 10 < \zeta^3 > + \ldots) \tag{5.12}$$

As mentioned already in Sect. 5.1 the expectation value of ζ^n is a function of J, $v + \frac{1}{2}$, (B_e/ω_e), and a_i's (SCH 61). The result for the expectation value is then:

$$< R^{-3} >_v = R_e{}^{-3}(1 + 9a_1(B_e/\omega_e)\,(v + \tfrac{1}{2}) + 12(B_e/\omega_e)\,(v + \tfrac{1}{2}) + \\ + O[(B_e/\omega_e)^2]) \tag{5.13}$$

The terms of second and higher order in (B_e/ω_e) may be neglected. The value of $d_T(nuclear)$ is calculated from the Eqs. (5.11) and (5.13) for the ground vibrational state. The results are given in Table 5.6. The term $d_T(electron\ coupled)$ represents the tensorial contribution of the electron coupled spin-spin interaction, which is very small compared with the nuclear spin-spin interaction. However, for the molecules HBr and HI its contribution is not negligible as the results given in Table 5.6 show. This is in contrast with the results for the molecules HF (MUE 70, LEE 71) and HCl (KAI 70, Lee 71), where $d_T(exp)$ equals $d_T(nuclear)$.

The scalar contribution of the electron coupled spin-spin interaction has been assumed equal to zero in fitting the spectra. In view of the fact that the spectra fit very well (Chap. 4), this assumption is valid within the present accuracy.

TABLE 5.6 Experimental values of the spin-spin coupling constant d_T(exp) compared with the calculated value of d_T(nuclear) from Eq. (5-11). All numbers are in kHz.[1]).

molecule	d_T(exp)	d_T(nuclear)
$H^{79}Br$	10.03(21)	10.49
$H^{81}Br$	10.89(21)	11.31
$D^{79}Br$	1.59(24)	1.60
$D^{81}Br$	1.74(24)	1.73
$H^{127}I$	5.51(10)	5.76

[1] The used nuclear g-factors (FUL 65) are:
$g(H) = 5.58556$, $g(D) = 0.8565$, $g(^{79}Br) = 1.4037$, $g(^{81}Br) = 1.51305$, and $g(^{127}I) = 1.123$.

5.7 CALCULATIONS

a Ab initio calculations

In the foregoing sections a number of molecular quantities for the equilibrium internuclear distance R_e have been determined. These molecular quantities give the possibility to check ab initio calculations for the molecules HBr and HI. To our knowledge such ab initio calculations have not been done until now. But these calculations can be expected after the successful ab initio studies of HF and HCl (MCL 67, BEN 69).

Failing these ab initio calculations for HBr and HI one used models and simplified calculations with molecular orbitals in order to obtain more comprehension of the molecular structure.

b Ionic model

Debije (DEB 29) has developed an ionic model in order to explain and predict the electric dipole moments of polar diatomic molecules. In this model each ion is polarized by the electrostatic field of the other one, and the dipole moment $\mu(R)$ is given by:

$$\mu(R) = eR\left[1 - \frac{(\alpha_1 + \alpha_2)R^3 + 4\alpha_1\alpha_2}{R^6 - 4\alpha_1\alpha_2}\right], \qquad (5.14)$$

where the quantities α_1 and α_2 are the dipole polarizabilities of ions 1 and 2 The internuclear distance is generally taken to be the equilibrium distance R_e

Rittner (RIT 51), De Wijn (WIJ 66), and Van Wachem (WAC 67) have used this model for the alkali-halides with success The result for the alkali-halides is that the polarizability of the alkali ion in a molecule is roughly that of the free alkali ion, but the polarizability of the halide ion is considerably smaller than that of the free halide ion (Table 5 7)

The values of the dipole moment at the distance R_e are for the hydrogen-halides $\mu_e(HF) = 1\ 7965$ D (MUE 70), $\mu_e(HCl) = 1\ 0933$ (KAI 70), $\mu_e(HBr) = 0\ 8165$ D (present work), $\mu_e(HI) = 0\ 4483$ D (present work) Assuming that the polarizability of the hydrogen ion in the hydrogen-halides equals zero, then we can calculate the polarizability of the halide ion from Eq (5 14) The results are given in Table 5 7 Comparing the polarizabilities of the halide ions in the hydrogen-halides with those in the alkali-halides, we see roughly the same increase of the polarizability in the series F, Cl, Br and I

TABLE 5 7 Polarizabilities of the halide ions

ion	polarizability of the free halide-ion[a] (10^{-24} cm^3)	polarizability of the halide-ion given as percentage of the polarizability of the free halide-ion in alkali-halides[b]	hydrogen-halides
F^-	1 04	54%	43%
Cl^-	3 66	61%	46%
Br^-	4 77	65%	52%
I^-	7 10	68%	55%

[a] Reference WIJ 66, [b] Reference WAC 67

The polarizability of a free halide ion is α De Wijn (WIJ 66) has suggested for the alkali-halides to substitute $\alpha_2 - (2/3)\alpha$ in stead of $\alpha_2 - \alpha$, since only four of the six outer electrons in the halide ions are polarizable This explains roughly the results for the alkali-halides, but not for the hydrogen-halides

Because the ionic model fails to explain the dipole moment of the hydrogen-halides, we will not apply it to the electric field gradient in these molecules The cause of this failure is the fact that the hydrogen-halides are not fully ionic molecules This appears, for instance, from the value of the ionic character of these molecules

c Ionic character

Starting from a molecular orbital which is a linear combination of atomic

orbitals of the two atoms in the molecule, Gordy and Cook (GOR 70, p 617) determined from the dipole moment the ionic character i_c of the hydrogen-halides:

$$i_c e R_e - \mu_{obs} + |\mu_s| + |\mu_{ind}| \qquad (5\ 14)$$

where μ_{obs} is the observed dipole moment, and μ_s and μ_{ind} represents the contribution to the dipole moment owing to the charge overlap and to the induced dipole moment, respectively Gordy and Cook obtained the following results: i_c = 0 82, 0 42, 0 34, and 0 26 for HF, HCl, HBr, and HI, respectively.

Assuming that the field gradient q at the halide nucleus arises from atomic p-electrons only, the ionic character of the hydrogen-halides has been determined also from the observed quadrupole coupling constants at the halide nuclei (GOR 70, p 576) The results are roughly the same as those obtained from the dipole moments.

The value of the quadrupole coupling constant $(eqQ)_D$ is 354 kHz, 187 kHz, and 146 kHz for DF (MUE 70), DCl (KAI 70), and DBr (present work), respectively. The ratio $(eqQ)_D/i_c$ turns out to be a constant equal to 440 kHz. With the value of i_c — 0.26 for DI, the $(eqQ)_D$ for DI can be predicted to be about 114 kHz.

TABLE 5 8 Spin-rotation coupling constants (in kHz) at the halide nucleus of the hydrogen-halides

molecule	C (v = o)	C_e	$C_e^{(n)}$	$C_e^{(e)}$
HF[a]	307 6	285	—55 2	340
$H^{35}Cl$[b]	53 9	51 6	— 2 1	54
$H^{79}Br$[c]	290 8	280	— 3 9	284
HI[c]	351 1	340[d]	— 2 1	342

[a] Reference MUE 70, [b] Reference KAI 70, [c] present work, [d] estimated value

In Table 5 8 the electronic part of the spin-rotation coupling constant $C_e^{(e)}$ of the halide nucleus is given for the hydrogen-halides at the internuclear distance R_e It is a complicated function of the electronic distribution in the molecule as can be seen from the expression for $C_e^{(e)} = (M_{aa})_e^{(e)}$ in Table 3.1 A model in terms of the ionic character or of an other quantity is not present to explain the values of the electronic part of the spin-rotation coupling constants.

Bab 65 H. J BABROV, A. L. SHABOTT and B. S. RAO, *J. Chem. Phys.* **42** (1965) 4124.

Bau 66 R. J. BAUER, M. COHN, J. H COTTON and R F. PACKARD, *Proc. IEEE* **54** (1966) 595.

Bec 70 E. J. BECKLAKE, C. D. PAYNE and B. E. PREWER, *J. Phys. D Appl. Phys.* **3** (1970) 473.

Ben 64 W. BENESCH, *J. Chem. Phys.* **40** (1964) 422.

Ben 69 C. F. BENDER and E. R. DAVIDSON, *Phys. Rev.* **183** (1969) 23.

Blu 68 H. BLUYSSEN, *thesis*, Fysisch Laboratorium, Nijmegen (1968).

Bon 70 P. A. BONCZYK, *Phys. Let.* **31A** (1970) 509.

Bri 66 N. BRIDGE and A. BUCKINGHAM, *Proc. Roy. Soc.* A **295** (1966) 334.

Bro 66 H H. BROWN and J. G. KING, *Phys. Rev.* **142** (1966) 53.

Bur 59 C. BURRUS, *J. Chem. Phys.* **31** (1959) 1270.

Bur 64 C. A. BURRUS, *Solid-St. Electron.* **7** (1964) 219.

Coh 63 M. COHN, F. WENTWORTH and J. WILTSE, *Proc. IEEE* **51** (1963) 1227.

Cor 70 V. J. CORCORAN, R E. CUPP, J. J. GALLAGHER and W. T. SMITH, *App. Phys. Let.* **16** (1970) 316.

Cot 63 J. M COTTON, *IEEE Tr. MTT* **11** (1963) 385.

Cow 56 M. COWAN and W. GORDY, *Phys. Rev.* **104** (1956) 551.

Cup 70 R. E. CUPP, V. J. CORCORAN and J. J. GALLAGHER, *IEEE J. Quan. Elec.* **QE-6** (1970) 160.

Deb 29 P. DEBIJE, '*Polar Molecules*', Dover Publications (1929).

Dij 68 F. A. VAN DIJK and A. DYMANUS, *Chem. Phys. Let.* **2** (1968) 235.

Dij 69 F. A. VAN DIJK and A. DYMANUS, *Chem. Phys. Let.* **4** (1969) 170.

Dij 67 F. A. VAN DIJK, *Monograph* **5**, Atomic and Molecular Research Group, Katholieke Universiteit, Nijmegen (1967).

Dij 69a F. A. VAN DIJK, *Quarterly Report* **24**, Atomic and Molecular Research Group, Katholieke Universiteit, Nijmegen (1969).

Dij 70 F. A. VAN DIJK, *Quarterly Report* **27**, Atomic and Molecular Research Group. Katholieke Universiteit, Nijmegen (1970).

Dre 69 H. D. DREW and A. J. SIEVERS, *App. Opt.* **8** (1969) 2067.

Dym 66 A. DYMANUS, *Monograph No* **1**, Atomic and Molecular Research Group, Katholieke Universiteit, Nijmegen (1966).

Edm 60 A R. EDMONDS, '*Angular Momentum in Quantum Mechanics*', Princeton University Press, Princeton, New Jersey (1960).

Ful 65 G. H. FULLER and V. W. COHEN, '*Nuclear Moments, Appendix I to Nuclear Data Sheets*', Oak Ridge Nat. Lab. (1965).

Gor 54 W. GORDY and C. H. BURRUS, *Phys. Rev.* **93** (1954) 419.

Gor 70 W. GORDY and R. L. COOK, '*Microwave Molecular Spectra*', Interscience Publishers, New York (1970).

Gus 70 B. P. GUSTAFSON and B. S. RAO, *Can. J. Phys.* **48** (1970) 330.

Heb 69 A. J. HEBERT and K. STREET, *Phys. Rev.* **178** (1969) 205.

Hel 69 P. HELMINGER and W. GORDY, *Phys. Rev.* **188** (1969) 100.

Hel 70 P. HELMINGER, F. C. DELUCIA and W. GORDY, *Phys. Rev. Let.* **25** (1970) 1397.

Her 50 G. HERTZBERG, '*Spectra of Diatomic Molecules*', Van Nostrand Company, Inc. New York (1950).

Hir 65 J. HIRSCHFELDER, C. CURTISS and R. BIRD, '*Molecular Theory of Gases and Liquids*', John Wiley, New York (1965).

Hui 66a C. HUISZOON and A. DYMANUS, *Phys. Let.* **21** (1966) 164.

Hui 66b C. HUISZOON, *thesis*, Fysisch Laboratorium, Nijmegen (1966).

Hui 71 C HUISZOON, *Rev. Sci. Inst.* **42** (1971) 477.

Hur 71 S. C. HURLOCK, R. M. ALEXANDER, K. N. RAO and S. N. DRESKA, *J. Mol. Spect.* **37** (1971) 373.

Jon 64a G. JONES and W. GORDY, *Phys. Rev.* **135** (1964) A295.
Jon 64b G. JONES and W. GORDY, *Phys. Rev.* **136** (1964) A1229.
Jud 63 B. R. JUDD, '*Operator Techniques in Atomic Spectroscopy*', Mc Graw-Hill Book Company, Inc., New York (1963).
Kai 70 E. W. KAISER, *J. Chem. Phys.* **53** (1970) 1686.
Kel 53 F. L. KELLER and A. H. NIELSEN, *Phys. Rev.* **91** (1953) 209.
Kne 69 F. KNEUBÜHL, *App. Opt.* **8** (1969) 505.
Lan 51 LANDOLT-BORNSTEIN, *Zahlenwerte und Funktionen Vol. I, Part 3* (Springer, Berlin 1951).
Lee 67 F. H. DE LEEUW, *Quarterly Report* **16**, Atomic and Molecular Research Group, Katholieke Universiteit, Nijmegen (1967).
Lee 70 F. H. DE LEEUW and A. DYMANUS, *Chem. Phys. Let.* **7** (1970) 288.
Lee 71 F. H. DE LEEUW, *thesis*, Fysisch Laboratorium, Nijmegen (1971).
Lut 70 O. LUTZ, *Phys. Let.* **31A** (1970) 384.
Mar 67 D. H. MARTIN, '*Spectroscopic Techniques*', North-Holland Publishing Company, Amsterdam (1967).
Mcc 67 M. MCCOLL, M. F. MILLEA, J. MUNUSHIAN and D. F. KYSEK, *Proc. IEEE* **55** (1967) 2169.
Mcl 67 A. D. MCLEAN and M. YOSHIMINE, *J. Chem. Phys.* **47** (1967) 3256.
Mer 63 R. MEREDITH and F. L. WARNER, *IEEE Tr. MTT* **11** (1963) 397.
Mue 68 J. MUENTER, *J. Chem. Phys.* **48** (1968) 4544.
Mue 70 J. MUENTER and W. KLEMPERER, *J. Chem. Phys.* **52** (1970) 6033.
Ohl 59 R. S. OHL, P. P. BUDENSTEIN and C. A. BURRUS, *Rev. Sci. Instr.* **30** (1959) 765.
Ove 68 P. A. M. VAN OVERBEEK, *Quarterly Report* **18**, Atomic and Molecular Research Group, Katholieke Universiteit, Nijmegen (1968).
Ove 68a P. A. M. VAN OVERBEEK and F. A VAN DIJK, *Quarterly Report* **20**, Atomic and Molecular Research Group, Katholieke Universiteit, Nijmegen (1968).
Pay 70 C. D. PAYNE and B. E. PREWER, *Rad. and Elec. Engineer*, **39** (1970) 167.
Put 65 E. H. PUTLEY, *App. Opt.* **4** (1965) 649.
Ram 56 N. F. RAMSEY, '*Molecular Beams*', Oxford University Press, Oxford (1956).
Ram 61 N. F. RAMSEY, *Am. Scientist* **49** (1961) 509.
Ran 65 D. H. RANK, U. FINK, and T. A. WIGGINS, *J. Mol. Spect.* **18** (1965) 170.
Ran 65a D. H. RANK, B. S. RAO, and T. A. WIGGINS, *J. Mol. Spect.* **17** (1965) 122.
Rao 68 B. S. RAO and L. H. LINDQUIST, *Can. J. Phys.* **46** (1968) 2739.
Rit 51 E. S. RITTNER, *J. Chem. Phys.* **19** (1951) 1030.
Rob 69 W. H. ROBINETTE and R. B. SANDERSON, *App. Opt.* **8** (1969) 711.
Rot 59 ROTENBERG, BIVINS, METROPOLIS and WOOTON, '*The 3-j and 6-j symbols*', Technology Press, M.I.T. Cambridge, Mass. (1959).
Sch 61 C. SCHLIER, *Fortschr. Phys.* **9** (1961) 455.
Sch 67 L. SCHARPEN, J. MUENTER and V. LAURIE, *J. Chem. Phys.* **46** (1967) 2431.
Tha 61 P. THADDEUS and L. KRISHER, *Rev. Sci. Instr.* **32** (1961) 1083.
Tha 64 P. THADDEUS, L. KRISHER and J. LOUBSER, *J. Chem. Phys.* **40** (1964) 257.
Tip 70 R. H. TIPPING and R. M. HERMAN, *J. Mol. Spect.* **36** (1970) 404.
Tow 55 C. H. TOWNES and A. L. SCHAWLOW, '*Microwave Spectroscopy*', McGraw Hill Book Comp., New York (1955).
Ver 69 J. A. T. VERHOEVEN, *thesis*, Fysisch Laboratorium, Nijmegen (1969).
Wac 67 R. VAN WACHEM, *thesis*, Fysisch Laboratorium, Nijmegen (1969).
Web 68 D. U. WEBB and K. N. RAO, *J. Mol. Spect.* **28** (1968) 12.
Wen 64 F WENWORTH, J. DOZIER and J. RODGERS, *Microwave J.* **7** (1964) 69.
Wij 66 H. W. DE WIJN, *J. Chem. Phys.* **44** (1966) 810.
Zah 24 C ZAHN, *Phys. Rev.* **24** (1924) 400.
Zui 69 B. ZUIDBERG, *Quarterly Report* **24**, Atomic and Molecular Research Group, Katholieke Universiteit, Nijmegen (1969).

SAMENVATTING

In dit proefschrift is de uitbreiding van de millimeter golf spectrometer gebouwd door Huiszoon (1966) tot het submillimeter golflengte gebied beschreven. De spectrometer heeft een hoog oplossend vermogen dat te danken is aan het feit dat de molekulen die de straling absorberen, bijna loodrecht gericht zijn op de voortplantingssnelheid van de straling. Hierdoor werd de Doppler verbreding van de spectraallijnen sterk gereduceerd. De gerichte molekulaire bundel werd verkregen door de molekulen door een met vloeibare stikstof gekoeld diafragma te sturen (Hoofdstuk 1).

De submillimeter straling werd verkregen uit een harmonische generator en gedetecteerd met een harmonische mixer. De harmonische generator en mixer bevatten beide een puntcontact diode, en werden elk afzonderlijk aangedreven door een 4 of 3 millimeter golf klystron. De materialen waaruit de puntcontact dioden opgebouwd werden, verschilden echter in beide dioden. Ook de constructie van de mixer week af van die van de generator. Hoge frequentie stabiliteit van het signaal werd verkregen door het signaal klystron te koppelen aan een precisie standaard frequentie. Door een modulerende elektrische spanning op de parallelle platen van de absorptie cel aan te brengen kon fase gevoelige demodulatie van het geabsorbeerde signaal toegepast worden. De gevoeligheid van het detectie systeem werd berekend met behulp van het geabsorbeerde vermogen in rotatie overgangen van molekulen. De gevoeligheid van de puntcontact mixer-diode is vergeleken met die van de thermische en foto geleidende detectoren, beide met helium gekoeld (Hoofdstuk 2).

Met deze spectrometer werd een rotatie overgang van de molekulen DBr, HI en HBr gemeten respectievelijk bij 255, 385 en 500 GHz zonder en met uitwendig elektrisch veld. Voor DBr en HBr werden de metingen verricht voor de beide isotopische vormen van de broom kern. Het uitwendig elektrische veld werd verkregen door op een van de parallelle platen van de cel een gelijk spanning aan te brengen. Het elektrische veld tussen de platen werd geijkt met de goed bekende waarde van het dipoolmoment van OCS. De meetresultaten van de bovengenoemde rotatie overgangen zijn vermeld in Hoofdstuk 4. Het oplossend vermogen bij 500 GHz bedroeg bijna $1 : 10^6$. Dit is het beste oplossend vermogen ooit bereikt bij een zo hoge frequentie.

De waargenomen hyperfijn en Stark spectra werden geinterpreteerd met een standaard Hamiltoniaan. Met behulp van sferische operatortechnieken werden de Stark en hyperfijn opsplitsingen van de rotatie niveaus van een molekuul berekend in termen van het elektrische dipoolmoment en de koppelingskon-

stanten van het molekuul (Hoofdstuk 3) Uit de waargenomen spectra werden het elektrisch dipoolmoment en de koppelingskonstanten met hoge nauwkeurigheid bepaald De waarden verkregen in dit onderzoek werden zo mogelijk vergeleken met waarden verkregen uit eerder verricht onderzoek

In Hoofdstuk 5 werden de verkregen waarden voor het dipoolmoment en de koppelingskonstanten geanalyseerd Daartoe werd de vibratie afhankelijkheid van het dipoolmoment en de koppelingskonstanten bepaald Omdat de metingen alleen in de vibratie grondtoestand van de molekulen verricht werden, kon de vibratie afhankelijkheid niet rechtstreeks uit de metingen bepaald worden Door dezelfde grootheid te meten in twee isotopische vormen van het molekuul kan de vibratie afhankelijkheid ook goed bepaald worden Dit isotopische substitutie effekt werd gebruikt voor HBr en DBr, waarbij de waterstof kern in HBr vervangen werd door zijn isotoop Op deze wijze werden grootheden bepaald die betrekking hebben op de molekulaire struktuur bij de evenwichtsafstand van de twee kernen De molekulaire grootheden geven de mogelijkheid ab initio berekeningen aan HBr en HI te testen Tot op heden zijn deze berekeningen nog niet verricht Maar ze kunnen wel verwacht worden na de suksesvolle studies met molekulaire golffunkties over HF en HCl

STELLINGEN

I

De molekulaire golffunkties voor benzeen, zoals ze gegeven zijn door Gray, zijn niet de golffunkties behorende bij de gediagonaliseerde energie-matrix.

H. G. GRAY, „*Electrons and Chemical Bonding*", W. A. BENJAMIN, Inc. New York (1964).

II

De hoge frequenties, die Strauch en medewerkers verkregen hebben met de methode van submillimetergolf harmonische mixing, zijn onvoldoende aangetoond.

R. STRAUCH, R. MIESCH en R. CUPP, *IEEE Tr. on MTT* **13** (1965) 873.
D. WOODS en R. STRAUCH, *Proc. IEEE* **54** (1966) 673.
G. SCHULTEN en J. STOLL, *IEEE Tr. on MTT* **14** (1967) 60.

III

Bij ver infrarood technieken in spectroscopie wordt gewoonlijk gebruik gemaakt van amplitude modulatie door middel van mechanische onderbreking van de straling. Bij voorkeur dient deze onderbreking zo dicht mogelijk bij de stralingsbron plaats te vinden.

R. JOYCE en P. RICHARDS, *Phys. Rev.* **179** (1969) 375.

IV

De door Goodell gegeven analyse van het verschijnsel van de door zee gereflecteerde hemelstraling zal aan waarde winnen, als men zowel de anisotropie in het golfpatroon van het water als de helderheidsverdeling van de hemel in rekening brengt.

J. B. GOODELL, *App. Opt.* **10** (1971) 223.

V

De cosinus hoekverdeling voor de richting van de molekulen komend uit een opening met een dunne wand blijft ook gelden bij lage Knudsen getallen (vrije weglengte $\simeq$ diameter van opening).

R. STICKNEY, R. KEATING, S. YAMAMOTO en W. HASTINGS, *J. Vac. Sci. and Tech.* **4** (1967) 10.

VI

In Toennies' analyse van de molekulaire bundel metingen van botsingsdoorsneden voor overgangen tussen specifieke rotatie-toestanden van TlF met verschillende molekulen, waaronder CH_4 en NH_3, is bij de berekening van de inelastische botsingsdoorsnede met CH_4 de dipool-octupool interaktie ten onrechte niet meegenomen. Bij de berekening van de totale botsingsdoorsnede met NH_3 had behalve de waarde van de quantum mechanische botsingsdoorsnede ook de waarde van de integrale botsingsdoorsnede verkregen met de klassieke theorie opgenomen dienen te worden.

J. P. TOENNIES, *Zeitschrift für Physik* **193** (1966) 76.

VII

Het beginsel van de veranderlijkheid, zoals door Van den Berg uiteengezet voor de natuurwetenschappen, is wat de fysica betreft onjuist.

J. H. VAN DEN BERG, „*Metabletica van de materie*", Callenbach N.V., Nijkerk (1969).

VIII

Als de regering ernst wil maken met het bieden van inspraak aan de burgers, hoort zij in de op stapel staande hervorming van de bestuurlijke indeling van Nederland als uitgangspunt voorop te stellen, dat bestaande gemeenten zoveel mogelijk moeten worden gehandhaafd.

23 september 1971

F. A. VAN DIJK